WATER RESOURCES RESEARCH, VOL. 49, 1292–1313, doi:10.1029/2012WR012994, 2013

Effects of harvest on carbon and nitrogen dynamics in a Pacific Northwest forest catchment

Alex Abdelnour,[1] Robert B. McKane,[2] Marc Stieglitz,[1,3] Feifei Pan,[1,4] and Yiwei Cheng[1]

Received 23 September 2012; accepted 1 November 2012; published 6 March 2013.

[1] We used a new ecohydrological model, Visualizing Ecosystems for Land Management Assessments (VELMA), to analyze the effects of forest harvest on catchment carbon and nitrogen dynamics. We applied the model to a 10 ha headwater catchment in the western Oregon Cascade Range where two major disturbance events have occurred during the past 500 years: a stand-replacing fire circa 1525 and a clear-cut in 1975. Hydrological and biogeochemical data from this site and other Pacific Northwest forest ecosystems were used to calibrate the model. Model parameters were first calibrated to simulate the postfire buildup of ecosystem carbon and nitrogen stocks in plants and soil from 1525 to 1969, the year when stream flow and chemistry measurements were begun. Thereafter, the model was used to simulate old-growth (1969–1974) and postharvest (1975–2008) temporal changes in carbon and nitrogen dynamics. VELMA accurately captured observed changes in carbon and nitrogen dynamics before and after harvest. The interaction of hydrological and biogeochemical processes in the model provided a means for interpreting these changes. Results show that (1) losses of dissolved nutrients in the preharvest old-growth forest were generally low and consisted primarily of organic nitrogen and carbon; (2) following harvest, carbon and nitrogen losses from the terrestrial system to the stream and atmosphere increased as a result of reduced plant nitrogen uptake, increased soil organic matter decomposition, and high soil moisture; and (3) the rate of forest regrowth following harvest was lower than that after fire because post-clear-cut stocks and turnover of detritus nitrogen were substantially lower than after fire.

Citation: Abdelnour, A., R. McKane, M. Stieglitz, F. Pan, and Y. Cheng (2013), Effects of harvest on carbon and nitrogen dynamics in a Pacific Northwest forest catchment, *Water Resour. Res.*, *49*, 1292–1313, doi:10.1029/2012WR012994.

1. Introduction

[2] Harvest and fire are two disturbances that have impacted the life history of the vegetation growth in forests of the Pacific Northwest (PNW) [*Agee*, 1990, 1994; *Franklin and Forman*, 1987; *Stednick*, 1996; *Wright and Agee*, 2004; *Wright and Heinselman*, 1973]. Forest fire and harvest in the PNW have been found to increase water yield [*Amaranthus et al*., 1989; *Bosch and Hewlett*, 1982; *Helvey*, 1980; *Hibbert*, 1966], summer low flow [*Keppeler and Ziemer*, 1990; *Neary et al*., 2005], peak streamflow [*Beschta et al*., 2000; *Harr and McCorison*, 1979; *Ice et al*., 2004], stream nutrient concentrations [*Beschta*, 1990; *Sollins and McCorison*, 1981; *Sollins et al*., 1981; *Tiedemann et al*., 1988], greenhouse gas emissions [*Harmon et al*., 1990; *Turner et al*., 2003], and soil microbial activity [*Bormann et al*., 1968; *Grant et al*., 2007]. Forest fire and harvest have also been shown to reduce evapotranspiration [*Jones and Post*, 2004; *Jones*, 2000; *Ice et al*., 2004], plant nitrogen uptake, and forest productivity [*Sollins and McCorison*, 1981]. These changes to hydrological and biogeochemical dynamics affect ecosystem services relevant to human well-being, including provisioning of forest products, clean water, flood protection, greenhouse gas regulation, wildlife habitat, and others [*Millennium Ecosystem Assessment* 2005]. For informed management decisions to be made, it is therefore important to understand how historical natural and man-made disturbances affected long-term watershed hydrology, carbon and nitrogen dynamics, and vegetation recovery, so as to draw insights into the impact of future management on key ecosystem processes. Attempts at investigating the impact of forest disturbances have usually been addressed through paired-watershed experiments [*Harr and McCorison*, 1979; *Langford*, 1976; *Moore and Wondzell*, 2005; *Weber and Flannigan*, 1997] or model simulations [*Janisch and Harmon*, 2002; *Storck et al*., 1998; *Tague and Band*, 2000; *Wright et al*., 2002].

[3] A number of experimental paired-watershed studies have explored the impact of harvest on ecosystem dynamics in PNW forests. These experimental studies have been

[1]Department of Civil and Environmental Engineering, Georgia Institute of Technology, Atlanta, Georgia, USA.
[2]U.S. Environmental Protection Agency, Western Ecology Division, Corvallis, Oregon, USA.
[3]School of Earth Atmospheric Sciences, Georgia Institute of Technology, Atlanta, Georgia, USA.
[4]Department of Geography, University of North Texas, Denton, Texas, USA.

Corresponding author: A. Abdelnour, Department of Civil and Environmental Engineering, Georgia Institute of Technology, Atlanta, GA 30332-0355, USA. (abdelnouralex@gmail.com)

0043-1397/13/2012WR012994

conducted in places such as the H.J. Andrews Experimental Forest (HJA) in the western-central Cascade Mountains of Oregon, and the Alsea watershed study in coastal Oregon, among others. For example, (1) *Stednick* [2008] used long-term measurement of nutrient losses to the stream to explore the impact of forest harvest on water quality in three watersheds in coastal Oregon, and (2) *Sollins and McCorison* [1981] measured nitrogen concentration in a small experimental watershed in western Oregon to explore the impact of clear-cutting on nitrogen pools and losses. Nonetheless, the complexity of experimental ecosystem studies often prevents direct interpretation of relationships between responses and specific perturbations [*Grant et al*., 2008]. Moreover, difficulties in separating the effects of plant biomass removal from the effects of roads have been identified and known to impact experimental results [*Yanai et al*., 2003]. Furthermore, experimental studies are usually expensive, require a significant time commitment, and cannot be used alone to quantify the contribution of specific processes to specific observed biogeochemical responses [*Alila and Beckers*, 2001; *Giesen et al*., 2008; *Stednick*, 2008].

[4] Process-based ecohydrological models can help address this need by providing a whole-system synthesis of disparate data sets and by exploring underlying process-level controls on catchment hydrological and biogeochemical responses to disturbance. Models can isolate the effect of a "target" treatment factor from the effects of other factors that may be unavoidably altered within a single treatment [*McKane et al*., 1997]. A number of models have been used to test forest management treatment scenarios, reproduce historical disturbances, and simulate postdisturbance successional changes in carbon and nitrogen, among others. For example, (1) *Harmon and Marks* [2002] developed a carbon model STANDCARB to examine the effects of forest management treatments such as slash burning, partial harvest, and clear-cutting, among others, on plant and soil carbon pools in PNW forests; (2) *Wimberly* [2002] used a spatial simulation model of forest succession to mimic presettlement landscape dynamics in the Oregon Coast Range; and (3) *Peng et al*. [2002] used the CENTURY model [*Parton et al.*, 1992] to simulate the impact of different harvesting intensities and rotation lengths on the long-term carbon and nitrogen dynamics of boreal forests in central Canada. These and other simulation models have provided an effective tool to complement field research and to examine the integrated responses of watershed hydrology, ecology, and biogeochemistry to interacting stressors.

[5] However, existing process-based models have disadvantages. Many are too simple to capture the important process-level hydrological and biogeochemical controls on ecosystem responses to disturbance. At the other extreme, some models are so complex that they require forcing data that are often unavailable, are too computationally expensive to extrapolate local dynamics over large watershed areas, or require a high level of expertise to implement. There is therefore a need for a balanced approach, specifically, an accessible, spatially distributed, ecohydrological model that is both computationally efficient and relatively easy to implement for analyzing the potential effects of changes in climate, land use, and land cover on watershed hydrological and biogeochemical processes.

[6] We use such an ecohydrological model, Visualizing Ecosystems for Land Management Assessments (VELMA) [*Abdelnour et al*., 2011]), to investigate the response of PNW forests to harvest. Specifically, we apply the model to a small intensively studied catchment (watershed 10 (WS10)), where a stand-replacing fire occurred in 1525 and a 100% clear-cut in 1975. First, we calibrate the model to simulate the buildup of ecosystem C and N stocks from the onset of the stand-replacing fire of 1525–1969 the first year with available streamflow and C and N data. Thereafter, we explore the temporal changes in measured and unmeasured biogeochemical fluxes such as nutrient losses, soil heterotrophic respiration, and N_2-N_2O emissions, among others, for two periods of interest: (1) during old-growth condition when the ecosystem was relatively close to steady state (1969–1974) and (2) following the 1975 whole-catchment clear-cut (1975–2008). Section 2 describes the study site. Section 3 provides an overview of the VELMA modeling framework. Section 4 describes the simulation methods, the calibration, and the sensitivity analysis. Section 5 presents model results and discussion. Section 6 summarizes our major conclusions.

2. Site Description

[7] WS10 of the HJA is a small 10.2 ha catchment located in the western-central Cascade Mountains of Oregon, at latitude 44°15′N and longitude 122°20′W (Figure 1). WS10 has been the site of intensive research and manipulation by the U.S. Forest Service since the 1960s, mainly to study the effects of forest harvest on hydrology, sediment transport, and nutrient loss [*Dyrness*, 1973; *Fredriksen*, 1975; *Harr and McCorison*, 1979; *Jones and Grant*, 1996; *Rothacher*, 1965; *Sollins and McCorison*, 1981; *Sollins et al*., 1981].

[8] WS10 elevation ranges from 430 m at the stream gauging station to 700 m at the southeastern ridgeline. Near-stream and side-slope gradients are approximately 24° and 25°–50°, respectively [*Grier and Logan*, 1977; *Sollins et al*., 1981]. The climate is relatively mild with wet winters and dry summers [*Grier and Logan*, 1977]. Mean annual temperature is 8.5°C. Daily temperature extremes vary from 39°C in the summer to −20°C in the winter [*Sollins and McCorison*, 1981]. Mean annual precipitation is 2300 mm and falls primarily as rain between October and April [*Jones and Grant*, 1996]. Snow rarely persists longer than a couple of weeks and usually melts within 1–2 days [*Harr and McCorison*, 1979; *Harr et al*., 1982; *Jones*, 2000]. Soils are of the Frissel series, which are classified as Typic Dystrochrepts with fine loamy to loamy-skeletal texture [*Sollins et al*., 1981; *Vanderbilt et al*., 2003] and are generally deep and well drained [*Grier and Logan*, 1977].

[9] Two significant events determined the life history of the vegetation growth in WS10, a stand-replacing fire event in 1525 [*Wright et al*., 2002] and a man-made clear-cut in 1975 [*Sollins and McCorison*, 1981]. Prior to the 100% clear-cut in 1975, WS10 was a 450 year old forest dominated by Douglas-fir (*Pseudotsuga menziessii*), western hemlock (*Tsuga heterophylla*), and western red cedar (*Thuja plicata*) [*Grier and Logan*, 1977] reaching up to approximately 60 m in height, with rooting depths rarely exceeding 100 cm [*Santantonio et al*., 1977]. In the spring

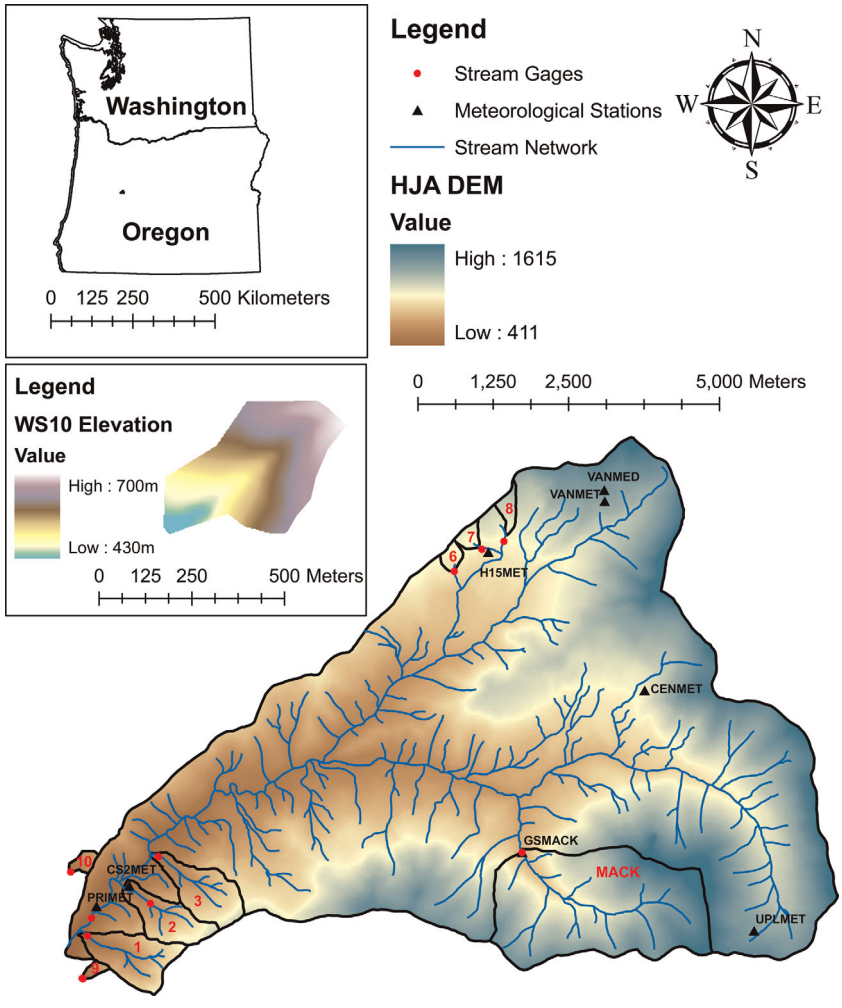

Figure 1. The study site is the WS10 of the HJA located in the western Cascade Range of Oregon. The red dots represent the locations of the stream gages. The black triangles represent the locations of the meteorological stations.

of 1975, WS10 was clear-cut. All trees and woody materials larger than 20 cm in diameter or 2.4 m in length, including many logs on the ground, were removed from the site. Large woody slash was disposed of without burning [*Gholz et al*., 1985]. Post-clear-cut residual plants consisted of understory shade tolerant vegetation and shrubbery, undamaged by harvest [*Gholz et al*., 1985]. Species such as vine maple (*Acer circinatum*), Pacific rhododendron (*Rhododendron maximum*), and chinkapin (*Castanopsis chrysophylla*) regenerated during the spring after logging. In 1976, 1 year after clear-cut, WS10 was planted with 2 year-old seedlings of Douglas-fir [*Gholz et al*., 1985]. The dominant vegetation of WS10 today is an approximately 35 year-old mixed Douglas-fir and western hemlock stand.

3. The Ecohydrological Model

[10] We have developed a spatially distributed ecohydrological model, VELMA, to simulate changes in soil water infiltration and redistribution, evapotranspiration (ET), surface and subsurface runoff, carbon and nitrogen cycling in plants and soils, and the transport of dissolved forms of carbon and nitrogen from the terrestrial landscape to streams. VELMA is designed to simulate the integrated responses of ecohydrological processes to multiple forcing variables, e.g., changes in climate, land use, and land cover. It is intended to be broadly applicable to a variety of ecosystems (forest, grassland, agricultural, tundra, etc.) and to provide a computationally efficient means for scaling up ecohydrological responses across multiple spatial and temporal scales: hillslopes to basins, and days to centuries. A detailed description of the biogeochemical component of VELMA is provided in Appendix A. [Note: The hydrological component of VELMA was presented in *Abdelnour et al*. [2011] and will not be described in the current manuscript.]

[11] The model uses a distributed soil column framework to simulate the movement of water and nutrients (organically bound carbon (C) and nitrogen (N) in plants and soils; dissolved inorganic nitrogen (DIN), dissolved organic nitrogen (DON), and dissolved organic carbon (DOC); and gaseous forms of C and N including CO_2, N_2O, and N_2)

within the soil, between the soil and the vegetation, and from the soil surface and vegetation to the atmosphere. The soil column model consists of three coupled submodels: (1) a *hydrological model* (Figure (A2)) that simulates vertical and lateral movement of water within soil, losses of water from soil and vegetation to the atmosphere, and the growth and ablation of the seasonal snowpack (the hydrological model is described in Appendix A of *Abdelnour et al*. [2011]); (2) a *soil temperature model* [*Cheng et al*., 2010] that simulates daily soil layer temperatures from surface air temperature and snow depth by propagating the air temperature first through the snowpack and then through the ground using the analytical solution of the one-dimensional thermal diffusion equation (equations (A1)–(A6)); and (3) a *plant-soil model* (Figure (A3)) that simulates ecosystem carbon storage and the cycling of C and N between a plant biomass layer and the active soil pools. Specifically, the plant-soil model simulates the interaction among aboveground plant biomass, soil organic carbon (SOC), soil nitrogen including dissolved nitrate (NO_3), ammonium (NH_4), and organic nitrogen, as well as DOC (equations (A7)–(A12)). Daily atmospheric inputs of wet and dry nitrogen deposition are accounted for in the ammonium pool of the shallow soil layer (equation (A13)). Uptake of ammonium and nitrate by plants is modeled using a Type II Michaelis-Menten function (equation (A14)). Loss of plant biomass is simulated through a density-dependent mortality. The mortality rate and the nitrogen uptake rate mimic the exponential increase in biomass mortality and the accelerated growth rate, respectively, as plants go through succession and reach equilibrium (equations (A14)–(A18)). Vertical transport of nutrients from one layer to another in a soil column is a function of water drainage (equations (A19)–(A22)). Decomposition of SOC follows first-order kinetics controlled by soil temperature and moisture content as described in the terrestrial ecosystem model (TEM) of *Raich et al*. [1991] (equations (A23)–(A26)). Nitrification (equations (A27)–(A30)) and denitrification (equations (A31)–(A34)) were simulated using the equations from the generalized model of N_2 and N_2O production of *Parton et al*. [1996, 2001] and *Del Grosso et al*. [2000].

[12] The soil column model is placed within a catchment framework to create a spatially distributed model applicable to watersheds and landscapes. Adjacent soil columns interact with each other through the downslope lateral transport of water and nutrients (Figure (A1)). Surface and subsurface lateral flow are routed using a multiple flow direction method [*Freeman*, 1991; *Quinn et al*., 1991]. As with vertical drainage of soil water, lateral subsurface downslope flow is modeled using a simple logistic function and corrected for the local topographic slope angle. Lateral transport of nutrients from one soil column to the subsequent soil column or toward the stream is simulated as a function of subsurface flow and nutrient-specific loss rates (equations (A35)–(A38)). Nutrients transported downslope from one soil column to another can be processed through the different C and N cycling submodels in that downslope soil column, or continue to flow downslope, interacting with other soil columns or ultimately discharging water and nutrients to the stream.

4. Simulation Methods

4.1. Data

[13] The model is forced with daily temperature, precipitation, and atmospheric nitrogen deposition. Observed daily temperature and precipitation data for the period 1 January 1969 to 31 December 2008 were obtained from the H.J. Andrews Long-Term Ecological Research (LTER) PRIMET, CS2MET, and H15MET meteorological stations located around WS10 [*Daly and McKee*, 2011] (see Figure 1). At the HJA, observed wet atmospheric nitrogen deposition is available approximately every 3 weeks, for the period 1968–2010, whereas observed dry atmospheric nitrogen deposition is available two to four times a year, for the period 1988–2010 [*Johnson and Fredriksen*, 2010]. However, for the purpose of our simulations, we will use the average annual value of the total wet and dry nitrogen deposition found by *Sollins et al*. [1980] (equation (A13)). *Sollins et al*. [1980] measured the average wet and dry nitrogen deposition in WS10 for the period 1973–1975 and found that annual N input in precipitation and dust was approximately 0.2 g Nm^{-2} yr^{-1}. This average annual value is then partitioned based on the ratio of daily precipitation to the average (1969–2008) annual precipitation.

[14] Observed data used for model calibration and validation include daily streamflow measured at the WS10 weir between 1969 and 2008 [*Johnson and Rothacher*, 2009], and NO_3, NH_4, DON and DOC losses to the stream measured for flow-weighted, composite samples collected approximately once every 3 weeks for the period 1978–2007, except DOC for which the period of record is 1992–2007 [*Johnson and Fredriksen*, 2011]. A 30 m resolution digital elevation model of the H.J. Andrews's WS10 [*Valentine and Lienkaemper*, 2005] was used to compute flow direction, delineate watershed boundaries, and generate a channel network. Each 30 m $\times$ 30 m soil column was divided into four layers and was assumed to have an average soil column depth to bedrock of 2 m [*Ranken*, 1974]. The dominant soil texture was specified as loam [*Ranken*, 1974]. Porosity, field capacity, and wilting point values were obtained following *Dingman* [1994].

4.2. Model Calibration and C and N "Spin-Up"

4.2.1. Hydrological Parameter Calibration

[15] *Abdelnour et al*. [2011] previously calibrated and validated VELMA's hydrological parameters to simulate pre-clear-cut and post-clear-cut temporal changes in WS10's streamflow. Specifically, model hydrological parameters such as the surface hydraulic conductivity, soil layer thicknesses, ET shape factor, and snowmelt parameters were calibrated to (1) reproduce the observed daily streamflow for the period 1969–2008, (2) capture the observed subsurface dynamics in WS10 (i.e., preferential lateral transport of water at the soil-bedrock interface [*Ranken*, 1974; *Van Verseveld et al*., 2008]), and (3) mimic the rapid runoff response to rainfall [*Kirchner*, 2003; *Ranken*, 1974]. Hydrological parameter names, values, and references can be found in Tables A1 and A2 in Appendix A of *Abdelnour et al*. [2011].

4.2.2. Biogeochemical Parameter Calibration

[16] A postfire "buildup" simulation was conducted for the period 1525–1968 (Figure 2) to identify, through

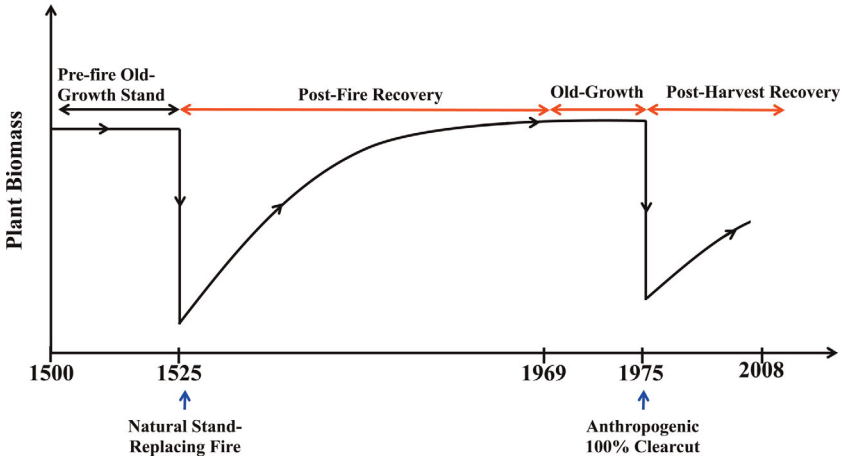

Figure 2. Schematics of the historical events that shaped the landscape in WS10: a natural stand-replacing fire that occurred in 1525 [*Wright et al*., 2002] and a 100% man-made clear-cut in 1975. The three periods of interest are as follows: (1) the postfire recovery period from 1525 to 1968, (2) the old-growth period (1969–1974) chosen at the end of the postfire recovery period where temperature and precipitation data are available to drive the model, and (3) the postharvest period from 1975 to 2008.

calibration, a single set of parameters that captures the accumulation of ecosystem C and N stocks following a stand-replacing fire in 1525 [*Grier*, 1975; *Grier and Logan*, 1977; *Wright et al*., 2002] to 1968. Daily temperature and precipitation drivers were constructed from a continuous loop of the available 1969–2008 observed climate station data. Typically, following stand-replacing fires, a large fraction of plant biomass is converted from live to dead matter [*Janisch and Harmon*, 2002], and a much smaller fraction is combusted as CO_2 [*Mitchell et al*., 2009]. Consequently, there is a correspondingly large increase in coarse detrital matter that decomposes slowly during the decades following fire [*Janisch and Harmon*, 2002]. Therefore, the postfire simulation was initialized by (1) reducing the initial live plant biomass value to 1% of its prefire old-growth value [*Wright et al*., 2002], (2) converting the dead plant biomass into detrital (soil) organic carbon [*Wright et al*., 2002], and (3) reducing the transpiration rate to zero initially, followed by an asymptotic increase to predisturbance values within 50 years [*Abdelnour et al*., 2011]. The 1525 initial conditions of plant biomass and SOC are 450 and 70,000 g Cm^{-2}, respectively. Model parameters such as plant uptake rate, plant mortality rate, and SOC decomposition rate were calibrated to achieve a biomass buildup trajectory (1525–1968) that passed through observed chronosequence data taken at WS10 and other PNW forest ecosystems [*Grier and Logan*, 1977; *Harmon et al*., 2004; *Janisch and Harmon*, 2002; *Smithwick et al*., 2002; *Sollins and McCorison*, 1981; *Sollins et al*., 1980] (Figure 3, Table 1). Calibration parameters determined from this postfire "buildup" simulation were then considered fixed for all subsequent WS10 simulations. A detailed description of the catchment biogeochemical dynamics associated with this calibration simulation is provided in section 5.1. Biogeochemical parameter names, values, and references are provided in Table B1.

4.3. Sensitivity Analysis

[17] We employ the method described by *McKane et al*. [1997] to conduct a sensitivity analysis of the model's calibrated parameters. This sensitivity analysis includes two parts. Part 1 examines the model's sensitivity to VELMA's most important hydrological and biogeochemical parameters. Specifically, we choose three hydrological parameters: surface hydraulic conductivity, lateral and vertical decay of the hydraulic conductivity with depth; and six biogeochemical parameters: loss rates for nitrate, ammonium, DON, and DOC, carbon decomposition rate into the DON pool, and average annual nitrogen deposition. Based on our experience with calibrating the model, these parameters were clearly the most important in affecting hydrological and biogeochemical outputs. We examined the model's sensitivity to each of these parameters individually by increasing or decreasing the calibrated value by 10% and 20%, then rerunning the model for all of the experimental treatments. We calculated the absolute differences between simulated and measured data for each of the five output variables (streamflow, NO_3, NH_4, DON, and DOC losses) for which high-quality observed data are available, in particular, observed stream flow and chemistry for WS10's preharvest (1969–1974) and postharvest (1975–2008) periods of record, and normalized it against the absolute differences between the original simulated results and the observed data. For each adjustment in a given variable, an error term was calculated to assess parameter sensitivity and used to help identify whether a given set of parameter values represents a best fit of the model to the observed data [*McKane et al*., 1997]:

$$E = \left[\sum_{i=1}^{5}\left(\frac{|S_i - O_i|}{|S_{i,o} - O_i|}\right)\right] \Big/ 5,$$

where E is the normalized absolute error, S_i is the simulated output (e.g., streamflow), O_i is the corresponding observed output, and $S_{i,o}$ is the original simulated output. If $E = 1$, the adjustment in variable did not result in any change in the absolute error. For $E > 1$, the adjustment in variable increased the absolute error, and, for $E < 1$, the adjustment

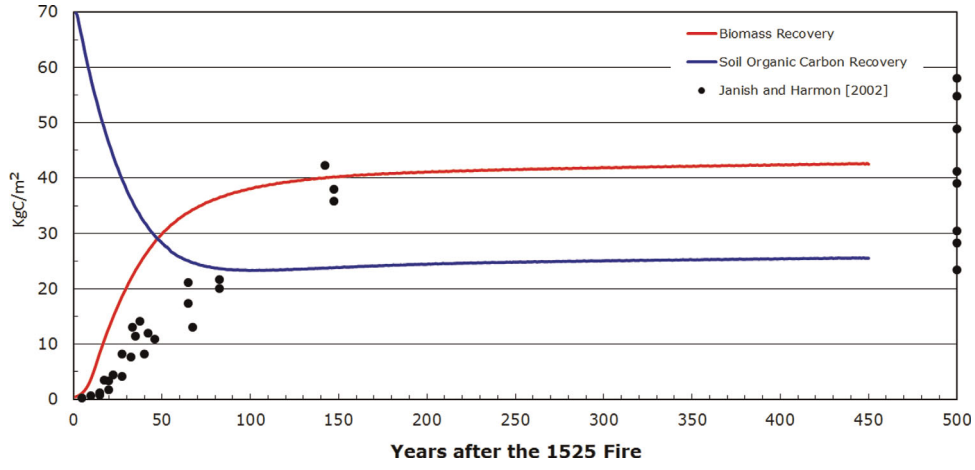

Figure 3. Simulated biomass (red line) and SOC (blue line) recovery after the 1525 stand-replacing fire. The black dots are the observed [*Janisch and Harmon*, 2002] accumulation of bole biomass (multiplied by 1.3 to get total plant biomass) for a 500 year chronosequence of 36 Pseudotsuga-Tsuga dominated forest stands in southwestern Washington State. The *x* axis is years since disturbance or age of the stand.

in variable decreased the absolute error. Part 2 of our sensitivity analysis examined how the overall error term changes when VELMA is calibrated to favor alternative flow pathways. The model is currently optimized for deep-flow paths [*Abdelnour et al*., 2011], those favoring rapid vertical flow and subsequent lateral flow along the soil-bedrock interface to the stream, that *Ranken* [1974], *Van Verseveld et al*. [2008], and *Kirchner* [2003] identified through their experimental studies as the predominant flow path in WS10. Alternatively, by changing soil layer thickness to have (1) equal soil layer thickness along the soil profile, which favors deep flow and slow runoff response to rainfall, or (2) a geometric progression of soil layer thickness along the soil profile, which favors shallow subsurface runoff and deep storage of water, we evaluated how well such a parameterization compares to the current one that is more consistent with available experimental data. Results of the sensitivity analysis showed that, for both Parts 1 and 2 of the sensitivity analysis, all of the *E* calculated are greater than 1.0 (Table 2 and Figure 4), indicating that the current model calibration provides the best fit to the measured data.

4.4. Pre-Clear-Cut and Post-Clear-Cut Simulations

[18] (1) *A pre-clear-cut "old-growth" simulation* was conducted for the period 1969–1974 (Figure 2) to explore daily, seasonal, and annual changes in C and N dynamics when the ecosystem was close to steady state conditions

Table 1. Comparison of the Postfire Simulation Results, for the Period 1960–1968, When the Ecosystem Is Considered in Steady State (i.e., Old-Growth Condition) Against Observed Old-Growth Values at Other PNW Forest

Output Parameter	Simulated Mean Value	Simulated Range of Values	Observed Mean Value	Observed Range of Values	Reference
DIN loss (g Nm^{-2} yr^{-1})	0.03	0.012–0.05	0.040	0.019–0.06	*Sollins et al*. [1980]
DON loss (g Nm^{-2} yr^{-1})	0.12	0.09–0.17	0.09	0.075–0.11	*Sollins and McCorison* [1981]
DOC loss (g Cm^{-2} yr^{-1})	1.8	1.3–2.4	3.18	2.0–4.3	*Sollins and McCorison* [1981]
			3.000	1.0–10.0	*Grier and Logan* [1977]
Plant biomass (g Cm^{-2})	42,500	42,300–42,600	39,807	34,800–44,800	*Harmon et al*. [2004]
			45,500	14,700–60,600	*Smithwick et al*. [2002]
			43,500		*Grier and Logan* [1977]
SOC (g Cm^{-2})	25,600	25,500–25,800	22,092	20,600–23,600	*Harmon et al*. [2004]
			19,000		*Grier and Logan* [1977]
			39,600		*Means et al*. [1992]
			27,500	7500–50,000	*Smithwick et al*. [2002]
Total carbon storage (g Cm^{-2})	68,100	67,800–68,400	61,899	56,600–67,700	*Harmon et al*. [2004]
			62,400		*Grier and Logan* [1977]
Heterotrophic soil respiration (g Cm^{-2} yr^{-1})	488	457–549	577	479–675	*Harmon et al*. [2004]
Denitrification rate (g Nm^{-2} yr^{-1})	0.05	0.04–0.06	0.04	0.03–0.09	*Schmidt et al*. [1988]
			0.013	0.008–0.021	*Binkley et al*. [1992]
NPP (g Cm^{-2} yr^{-1})	498	463–563	597	453–741	*Harmon et al*. [2004]
			544		*Grier and Logan* [1977]
NEP (g Cm^{-2} yr^{-1})	9	5–10	20	−116–156	*Harmon et al*. [2004]
			44		*Grier and Logan* [1977]

Table 2. Normalized Absolute Errors for Various Adjustments of Hydrological and Biogeochemical Parameters

Sensitivity Analysis	Hydrological Parameters			Biogeochemical Parameters					
	K_s	F_v	f_l	qf_{NH_4}	qf_{NO_3}	qf_{DON}	qf_{DOC}	q	n_{in}
20% increase	1.3	1.03	1.2	1.1	1.2	1.12	1.01	1.7	1.005
10% increase	1.05	1.02	1.04	1.0	1.03	1.01	1.0	1.5	1.0
10% increase	NaN	NaN	NaN	1.0	1.0	1.0	1.0	1.01	1.0
20% increase	NaN	NaN	NaN	1.1	1.0	1.03	1.0	1.2	1.003

[*Sollins et al*., 1980]. Initial values of plant biomass, SOC, NH_4, NO_3, DON, and DOC pools were determined from the 1525–1968 postfire "buildup" simulation. A detailed description of the simulated nutrient flux dynamics for the old-growth period is provided in section 5.2.

[19] (2) *A post-clear-cut simulation* was conducted for the period 1975–2008 (Figure 2) to explore the impact of clear-cut on measured and unmeasured nutrient losses, soil heterotrophic respiration, and N_2-N_2O land-atmosphere emissions, among others. WS10 was a 100% clear-cut in the spring of 1975. All trees and woody materials larger than 20 cm in diameter or 2.4 m in length were removed from the site [*Sollins and McCorison*, 1981; *Halpern and Spies*, 1995]. The residual plants after the 1975 clear-cut consisted of understory shade tolerant plants and shrubbery, undamaged by harvest [*Grier and Logan*, 1977; *Gholz et al*., 1985]. To mimic the 1975 spring clear-cut, the initial live plant biomass value was reduced to 10% (approximately 4500 g Cm^{-2}) of its preharvest value [*Gholz et al*., 1985; *Lee et al*., 2002], and the SOC pool was increased by 10% to account for new inputs of dead roots and stumps (all other plant biomass was assumed to have been removed from the site as logs) [*Grier and Logan*, 1977; *Gholz et al*., 1985]. Plant transpiration rates were set to zero in 1975 and then increased asymptotically to predisturbance values within 50 years [*Abdelnour et al*., 2011]. A detailed description of the simulated nutrient flux dynamics for the postharvest period is provided in section 5.3.

5. Simulation Results and Discussion

[20] Results and discussion are generally presented in the following sequence: (1) changes in plant biomass and SOC, (2) changes in dissolved organic and inorganic C and N losses to the stream, (3) changes in gaseous losses of C and N to the atmosphere, and (4) changes in net primary production (NPP) and net ecosystem production (NEP).

5.1. Postfire "Buildup" of Ecosystem C and N Stocks (1525–1968)

5.1.1. Postfire Plant Biomass and SOC (1525–1968)

[21] Postfire simulated plant biomass increased from the 1525 value of 450 g Cm^{-2} at an average rate of 580 g Cm^{-2} yr^{-1} for the first 30 years and at a rate of 300 g Cm^{-2} yr^{-1} for the next 70 years (Figure 3). Thereafter, simulated plant biomass gradually leveled off, reaching an old-growth value of approximately 42,500 g Cm^{-2} after approximately 400 years. Postfire SOC decreased exponentially from the 1525 value of approximately 70,000 g Cm^{-2} as a result of high decomposition and low detritus input to the soil and reached its lowest level after about 100 years (Figure 3). At that point, regrowing plant biomass provided increasing amounts of detritus input to the soil, thereby replenishing the soil carbon pool. Soil carbon subsequently rose and stabilized at approximately 25,600 g Cm^{-2}, 300 years into the simulation (Figure 3). Simulated postfire recovery of plant biomass and SOC were generally consistent with observed successional changes in live and dead wood carbon stores in other forests of the PNW [*Janisch and Harmon*, 2002; *Spies et al*., 1988; *Turner et al*., 2004]. However, early (less than 100 years old) simulated successional rates of increase in plant biomass exceeded the reported observed values by *Janisch and Harmon* [2002] (see Figure 3). In Figure 3, observed data for all stands less than 100 years old were initiated after clear-cut, whereas all stands older than 100 years were after a stand-replacing fire. As a result, the difference between observed and simulated early successional plant biomass owe in part to the greater amount of nitrogen released from decomposing detritus following fire than after clear-cut.

5.1.2. Postfire Gaseous C and N Losses (1525–1968)

[22] Postfire simulated gaseous losses of C and N increased initially as a result of high SOC decomposition, high soil water content, and low levels of plant N uptake. Specifically, simulated soil heterotrophic respiration (R_h) followed a similar trajectory as SOC, peaking (1500 g Cm^{-2} yr^{-1}) in the year 1525 and then falling exponentially until reaching its lowest value 120 years after disturbance (Figure 5). Thereafter, R_h increased with increasing SOC and reached an equilibrium value of approximately 488 g Cm^{-2} yr^{-1}. Postfire simulated soil denitrification rates (N_2 and N_2O emissions to the atmosphere) increased rapidly and peaked 8 years after disturbance. Thereafter, soil denitrification decreased exponentially due to a reduction in soil nitrate availability and reached a steady state value of approximately 0.06 g Nm^{-2} yr^{-1}, approximately 300 years into the simulation. Similar results were found by *Turner et al*. [2003] who used the carbon cycle model, global biome model-biogeochemical cycle (BIOME-BGC), to explore the temporal dynamics of carbon fluxes in two western Oregon watersheds. *Turner et al*. [2003] found that R_h peaked (approximately 1300 g Cm^{-2} yr^{-1}) at the onset of the disturbance, then decreased exponentially, and reached equilibrium value (approximately 600 g Cm^{-2} yr^{-1}) within 200 years.

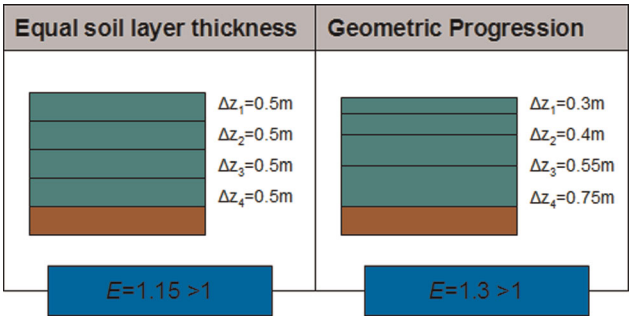

Figure 4. Normalized absolute errors for various adjustments of soil layer thickness.

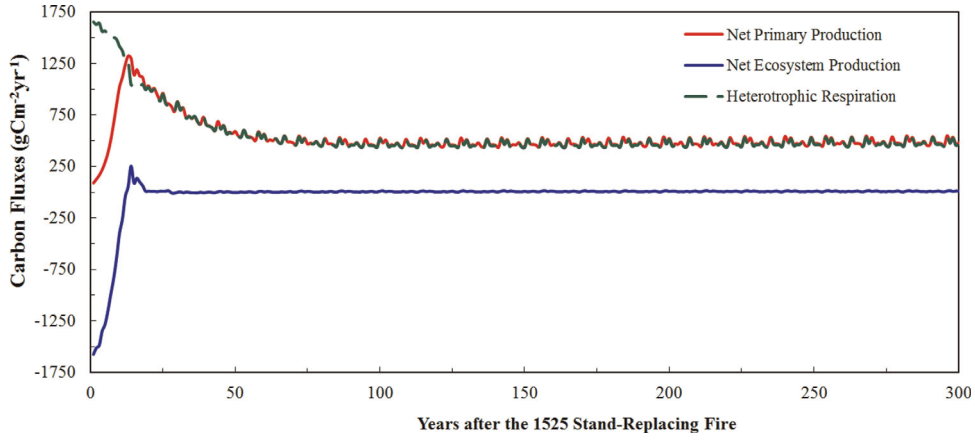

Figure 5. Simulated NPP (red line), NEP (blue line), and soil heterotrophic respiration (green dashed line) recovery after the 1525 stand-replacing fire. The *x* axis is years since disturbance or age of the stand.

5.1.3. Postfire NPP and NEP (1525–1968)

[23] As a result of vegetation removal and the large soil decomposition-driven losses of C as CO_2 to the atmosphere and as DOC to the stream, the initial 1525 postfire simulated value of NPP and NEP was 90 and −1500 g Cm^{-2} yr^{-1}, respectively (Figure 5). Thereafter, simulated NPP increased with increasing N availability in the soil, reached a peak value of approximately 1300 g Cm^{-2} yr^{-1} 14 years after fire, then decreased exponentially due to the decrease in N availability, and finally reached a stable value of approximately 500 g Cm^{-2} yr^{-1} within 200 years. Similarly, postfire simulated NEP increased with the rapid regrowth of plant biomass and became positive, peaking at approximately 150 g Cm^{-2} yr^{-1} after 15 years. Thereafter, NEP decreased exponentially, reaching a steady-state average equilibrium value of approximately 9 g Cm^{-2} after 200 years. Postfire changes in NPP and NEP are generally consistent with a variety of chronosequence observations and modeling studies (Figure 6) [e.g., *Luyssaert et al.*, 2008; *Turner et al.*, 2003; *Hicke et al.*, 2003; *Law et al.*, 2001; *Janisch and Harmon*, 2002, among others]. For example, *Turner et al.* [2003] used the BIOME-BGC model to analyze forest carbon dynamics in the HJA and found that (1) NPP was near zero early in succession, increased and reached 1200 g Cm^{-2} yr^{-1}, 15 years after disturbance, then decreased exponentially, and reached an equilibrium value of approximately 620 g Cm^{-2} yr^{-1} within 200 years; and (2) NEP was strongly negative (approximately −1300 g Cm^{-2} yr^{-1}) at the onset of the disturbance, peaked at approximately 700 g Cm^{-2} yr^{-1} 15 years after disturbance, then decreased exponentially, and reached an equilibrium value of approximately 20 g Cm^{-2} yr^{-1} within 200 years.

5.2. Old-Growth Biogeochemical Dynamics (1969–1974)

[24] At daily time scales, simulated nutrient losses were generally high in the wet season and low in the summer dry season. Specifically, simulated daily NH_4 losses averaged

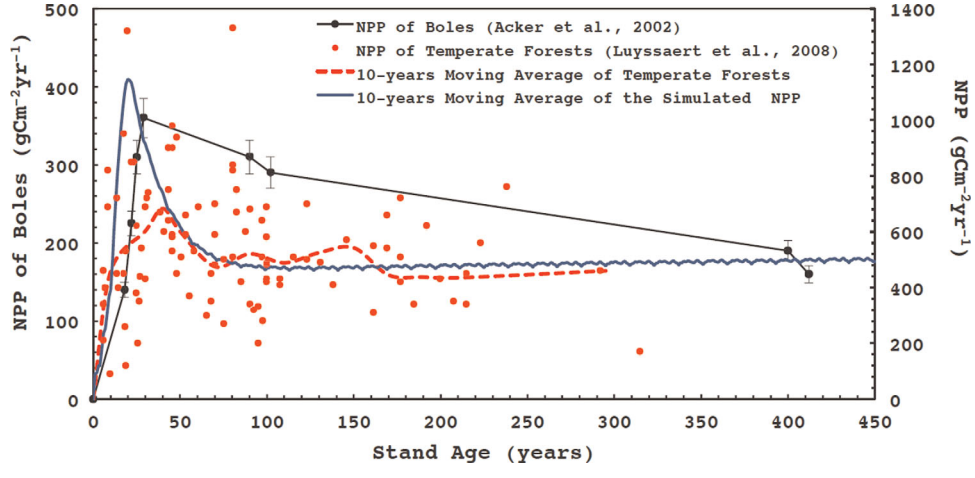

Figure 6. Comparison between the simulated postfire 10 year moving averages of ecosystem NPP (blue line) and the observed (1) NPP of temperate forests (red dots are individual forest stands sampled throughout the world; red dashed line is a 10 year moving average) [*Luyssaert et al.*, 2008] and (2) NPP of boles for PNW coniferous forests (black dots and solid black line) as a function of stand age (i.e., time after stand-replacing disturbance) [*Acker et al.*, 2002].

Table 3. Comparison of Simulation Results From the Old-Growth Simulation Against Observed Values at WS10 and Other Old-Growth PNW Forests

Output Parameter	Simulated Mean Value	Observed Mean Value	Reference
NH_4 loss (g Nm^{-2} yr^{-1})	0.023 (0.018–0.03)	0.01	*Vanderbilt et al*. [2003]
NO_3 loss (g Nm^{-2} yr^{-1})	0.008 (0.003–0.01)	0.01 (0.009–0.011)	*Martin and Harr* [1989]
		0.003	*Vanderbilt et al*. [2003]
DIN loss (g Nm^{-2} yr^{-1})	0.032 (0.02–0.04)	0.04 (0.01937–0.06)	*Sollins et al*. [1980]
DON loss (g Nm^{-2} yr^{-1})	0.14 (0.12–0.18)	0.089 (0.0745–0.1043)	*Sollins and McCorison* [1981]
DOC loss (g Cm^{-2} yr^{-1})	2.94 (1.7–4.54)	3.178 (2.015–4.34)	*Sollins and McCorison* [1981]
		3 (1–10)	*Grier and Logan* [1977]
$\frac{NH_4 loss}{NO_3 loss}$	3	2	*Vanderbilt et al*. [2003]
$\frac{NH_4 loss}{Total\ N\ loss}$	14%	18–33%	*Sollins and McCorison* [1981]
$\frac{DON\ loss}{Total\ N\ loss}$	81%	80%	*Vanderbilt et al*. [2003]
$\frac{DOC\ loss}{DON\ loss}$	21 (14–36)	21–52	*Cairns and Lajtha* [2005]
Q versus DON	$R^2 = 0.8$	$R^2 = (0.4–0.79)$	*Vanderbilt et al*. [2003]
Q versus NH_4	$R^2 = 0.6$	$R^2 = 0.51$	*Vanderbilt et al*. [2003]

0.06 mg Nm^{-2} d^{-1} and were strongly correlated to precipitation ($R^2 = 0.8$) and stream discharge ($R^2 = 0.6$). NH_4 losses peaked in fall and winter with the peaks in streamflow and reached 1.2 mg Nm^{-2} d^{-1}. Summer NH_4 losses were low, averaging 0.03 mg Nm^{-2} d^{-1}. Simulated daily NO_3 losses averaged 0.02 mg Nm^{-2} d^{-1} and were strongly correlated to streamflow ($R^2 = 0.7$) but weakly correlated to precipitation ($R^2 = 0.4$). Simulated NO_3 losses were largest (1) in the summer as a result of high nitrification rates and (2) in the fall at the onset of the rainy season when hydrological connectivity within hillslopes is reestablished and nutrients accumulated in soils during drier summer months are more readily flushed downslope [*Creed et al*., 1996; *Stieglitz et al*., 2003]. Simulated daily DOC and DON losses averaged 7.6 mg Cm^{-2} d^{-1}, and 0.5 mg Nm^{-2} d^{-1}, respectively, and were strongly correlated to stream discharge ($R^2 = 0.8$ and 0.9, respectively). DOC and DON losses peaked with peakflow, reaching 115.5 mg Cm^{-2} d^{-1} and 6.7 mg Nm^{-2} d^{-1}, respectively, and were largest in fall and winter. In the summer season, DOC and DON losses were minimal and averaged 0.8 mg Cm^{-2} d^{-1} and 0.05 mg Nm^{-2} d^{-1}, respectively. Similar results have been found by *Vanderbilt et al*. [2003], who analyzed long-term organic and inorganic nitrogen outputs in stream water in six watersheds at the HJA in Oregon. They found that NH_4, NO_3, and DON losses to the stream were correlated to stream discharge with a R^2 of 0.5, 0.5, and 0.8, respectively. Note that observed daily nutrient loss data for the period 1969–1975 were unavailable at WS10 for a comparison with our simulated daily values.

[25] On an annual basis, simulated losses of DIN (NH_4 and NO_3) averaged 0.03 g Nm^{-2} yr^{-1} with NH_4 losses being three times NO_3 losses to the stream (NO_3/NH_4 approximately 33%). Specifically, simulated annual NO_3 and NH_4 losses averaged 0.008 and 0.023 g Nm^{-2} yr^{-1}, respectively. Simulated annual DON losses averaged 0.14 g Nm^{-2} yr^{-1} and accounted for 81% of the nitrogen that reached the stream (DON/DIN = 4.4). Simulated annual DOC losses averaged 2.9 g Cm^{-2} yr^{-1} and ranged between 1.7 and 4.5 g Cm^{-2} yr^{-1}. These simulated old-growth nutrient fluxes were consistent with other studies of the biogeochemical dynamics of old-growth forests in the PNW (Table 3). For example, *Sollins and McCorison* [1981] measured nitrogen and carbon solution chemistry in WS10 before the 1975 clear-cut and found that, in an undisturbed watershed, NH_4 accounted for 18%–33% of total dissolved nitrogen, DON accounted for the rest, and NO_3 concentration was very low. Similarly, *Fredriksen* [1975] found that nitrogen losses in undisturbed forests are small and occur primarily as DON.

5.3. Postharvest Biogeochemical Dynamics (1975–2008)

[26] To explore the impact of the 1975 WS10 clear-cut on C and N dynamics, we conducted two simulations: a postharvest simulation for the period 1975–2008 (described in section 4.2) and a control simulation, over the same period, in which no vegetation is removed (i.e., soil and plant C and N dynamics are at steady state and similar to old-growth dynamics, Tables 1 and 3). Simulated post-clear-cut relative changes in C and N fluxes are presented in terms of the difference between the postharvest simulation values and the control simulation values.

5.3.1. Post-Clear-Cut Plant Biomass and SOC (1975–2008)

[27] Simulated post-clear-cut plant biomass increased rapidly at a rate of approximately 400 g Cm^{-2} yr^{-1} as a result of large early successional N uptake rates and N availability and reached a standing stock of 16,000 g Cm^{-2}, 30 years after disturbance. Simulated post-clear-cut SOC decreased as a result of high SOC decomposition and low detritus input into the soil. Simulated SOC reached 55% of its initial value (approximately 15,000 g Cm^{-2}) 30 years after clear-cut. Simulated recoveries of plant biomass and SOC were consistent with observed early successional changes in live and dead wood carbon stores in PNW forests [*Janisch and Harmon*, 2002; *Spies et al*., 1988]. However, post-clear-cut simulated successional rates of change in plant biomass and SOC exceeded the reported observed values by *Janisch and Harmon* [2002]. *Janisch and Harmon* [2002] found that live tree bole carbon stores increased after disturbance and reached approximately 7500 g Cm^{-2} (i.e., approximately 9500 g Cm^{-2} for total plant biomass), 30 years after disturbance. Moreover, *Janisch and Harmon* [2002] found that coarse woody detritus carbon stores decreased after clear-cut and reached 50% of its initial mass (approximately 2800 g Cm^{-2}), 30 years after disturbance. Nevertheless, *Janisch and Harmon* [2002] simulated old-growth values of live and dead carbon stores (31,900 and 7200 g Cm^{-2}, respectively) were generally at

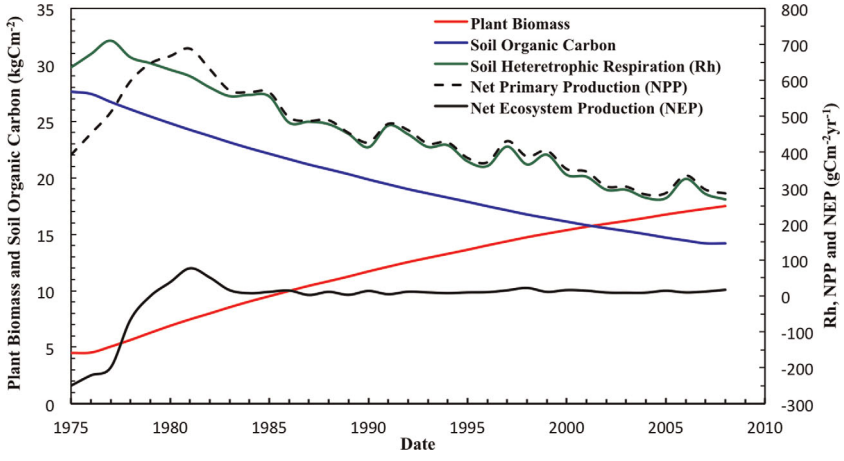

Figure 7. Simulated recovery of plant biomass (kg Cm^{-2}; red line), SOC (kg Cm^{-2}; blue line), NPP (g Cm^{-2} yr^{-1}; black dashed line), NEP (g Cm^{-2} yr^{-1}; black line), and soil heterotrophic respiration (g Cm^{-2} yr^{-1}; green line) after a 100% clear-cut in 1975. The *x* axis represents the 1975–2008 period of available precipitation and temperature data.

the lower end of the range reported for Oregon forests (29,500–58,500 g Cm^{-2} [*Grier and Logan*, 1977; *Harmon et al*., 2004] and 12,700–32,600 g Cm^{-2} [*Grier and Logan*, 1977; *Harmon et al*., 2004; *Means et al*., 1992]).

5.3.2. Post-Clear-Cut Dissolved C and N Losses (1975–2008)

[28] Post-clear-cut losses of dissolved inorganic N to the stream peaked a few years after disturbance as a result of high SOC decomposition, low levels of plant N uptake prior to significant reestablishment of plant biomass, and the increase in streamflow. Specifically, simulated annual NH_4 and NO_3 losses peaked 2 years after clear-cut and averaged 0.08 g Nm^{-2} yr^{-1} (fourfold higher than control values) and 0.9 g Nm^{-2} yr^{-1} (150-fold higher than control values), respectively, over the first 5 years. Thereafter, simulated annual NH_4 and NO_3 losses decreased as a result of a decreasing SOC pool and an increase in N uptake by plants and reached 0.015 g Nm^{-2} yr^{-1} (25% lower than control values) and 0.008 g Nm^{-2} yr^{-1} (10% lower than control values), respectively, 30 years after clear-cut. The simulated changes in NH_4 and NO_3 losses to the stream were consistent with the observed data at WS10 (see Figure 8 and Table 4) as well as previously published studies of biogeochemical dynamics in recently clear-cut old-growth forests [e.g., *Cairns and Lajtha*, 2005; *Sollins and McCorison*, 1981; *Fredriksen*, 1975]. For example, *Sollins and McCorison* [1981] found that NO_3 concentration increased as much as 100-fold, 7–18 months after the 1975 clear-cut of WS10. *Fredriksen* [1975] found that, following forest clear-cut at two experimental watersheds in western Oregon, sharp increases in stream N concentrations were attributed to decreased plant N uptake and increased detritus N subject to mineralization into ammonium. *Vitousek and Reiners* [1975] found that vegetation removal by fire or forest harvest results in an immediate but transient flush of N to streams, which is quickly followed by tight retention of N in young vigorously growing stands.

[29] Post-clear-cut simulated dissolved organic C and N losses to the stream were driven by high SOC decomposition and high subsurface flow. Specifically, simulated annual DON and DOC losses peaked 2 years after clear-cut and averaged 0.15 g Nm^{-2} yr^{-1} (approximately 20% higher than control values) and 3.2 g Cm^{-2} yr^{-1} (approximately 18% higher than control values) over the first 5 years, respectively. Thereafter, simulated annual DON and DOC losses decreased with decreasing SOC and averaged 0.07 g Nm^{-2} yr^{-1} (approximately 30% lower than control values) and 1.1 g Cm^{-2} yr^{-1} (approximately 35% lower than control values) 30 years after clear-cut, respectively. Changes in DON and DOC losses to the stream were consistent with the observed post-clear-cut nutrients dynamics in WS10 (see Figure 8 and Table 4) and other PNW forests. *Cairns and Lajtha* [2005] found that DON and DOC losses in young watersheds were approximately 30% and 25% higher than in old watersheds, respectively. *Sollins and McCorison* [1981] found that DOC concentrations were higher in the clear-cut watershed compared to the control watershed.

5.3.3. Post-Clear-Cut Gaseous C and N Losses (1975–2008)

[30] Post-clear-cut simulated gaseous losses of C and N increased as a result of high SOC decomposition, high soil water content, and low levels of plant N uptake prior to significant plant regrowth. Specifically, simulated annual denitrification rates and soil heterotrophic respiration (R_h) peaked 2 years after clear-cut and averaged 0.9 g Nm^{-2} yr^{-1} (approximately 13-fold higher than control values) and approximately 710 g Cm^{-2} yr^{-1} (30% higher than control values) from 1975 to 1980, respectively (Figure 7). Thereafter, simulated annual denitrification rates and R_h decreased with increasing plant biomass, increasing N uptake, and decreasing SOC and soil water content. By 2005, 30 years after clear-cut simulated annual denitrification rates and R_h averaged 0.07 g Nm^{-2} yr^{-1} (30% lower than control values) and 280 g Cm^{-2} yr^{-1} (40% lower than control values), respectively. The simulated changes in gaseous losses of C and N were consistent with previously published studies of biogeochemical dynamics in recently clear-cut old-growth forests. For example, *Grant et al*. [2007] used an ecosystem model *ecosys* [*Grant et al*.,

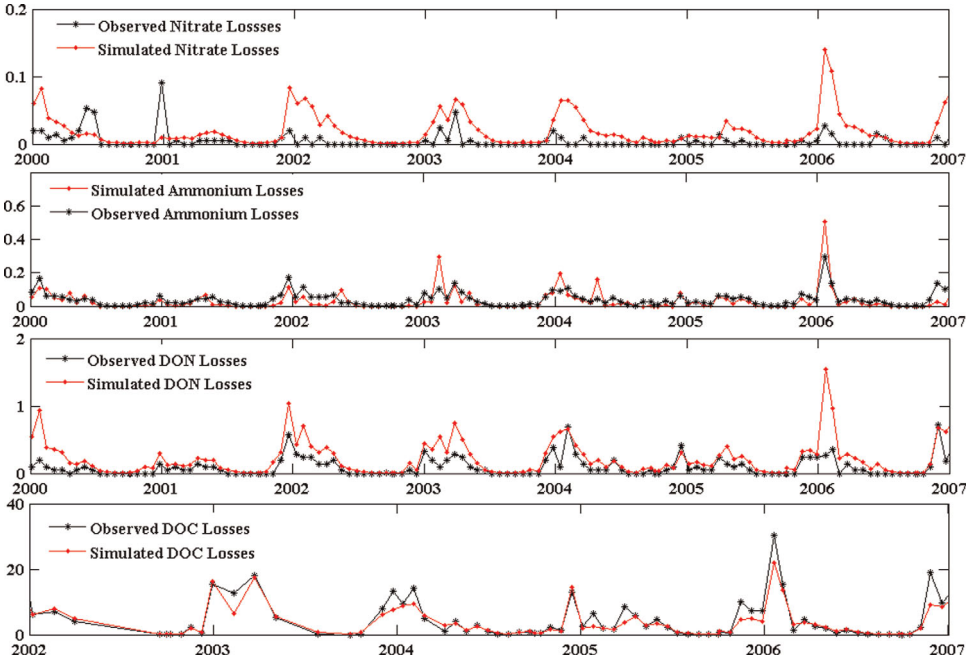

Figure 8. Simulated (red dots) versus observed (black dots) NO_3 (mg Nm^{-2}), NH_4 (mg Nm^{-2}), DON (mg Nm^{-2}), and DOC losses (mg Cm^{-2}) to the stream after the 1975 clear-cut of WS10 in the H.J. Andrews. The simulated values are averages over the same time interval as the observed values. The *x* axis represents the selected set of data between 2000 and 2007 for NO_3, NH_4, and DON losses and between 2002 and 2007 for DOC losses. The *y* axis represents the amount of daily losses that reaches the stream.

2001] to simulate the impact of clear-cutting on R_h in an old-growth forest of the PNW and found that R_h peaked (approximately 1200 g Cm^{-2} yr^{-1}) 2 years after clear-cut and then decreased and reached approximately 350 g Cm^{-2} yr^{-1}, 50 years after clear-cut. *Griffiths and Swanson* [2001] measured the microbiological characteristics of forest soils in recently harvested and old-growth Douglas-fir in the HJA and found that the denitrification rate increased six-fold 5 years after clear-cut, then decreased and was 20% lower than old-growth values, for a 40 year-old stand.

5.3.4. Post-Clear-Cut NPP and NEP (1975–2008)

[31] Post-clear-cut simulated NPP and NEP decreased from an old-growth value of 498 and 9 g Cm^{-2} yr^{-1} respectively, as a result of vegetation removal, and large decomposition-driven losses of C as CO_2 to the atmosphere and as DOC to the stream (Figure 7). Specifically, simulated annual NPP decreased by 45%, to approximately 390 g Cm^{-2} yr^{-1} at the onset of clear-cut, then increased with the rapid regrowth of plant biomass, and peaked (approximately 700 g Cm^{-2} yr^{-1}) 7 years after clear-cut. Thereafter, annual NPP decreased and reached an average value of approximately 300 g Cm^{-2} yr^{-1} (approximately 45% lower than control values), 30 years after clear-cut. Similarly, simulated annual NEP dropped to −250 g Cm^{-2} yr^{-1} at the onset of the clear-cut; peaked at 75 g Cm^{-2} yr^{-1} 7 years after disturbance as a result of rapid regrowth of plant biomass, high N uptakes, and a decrease in soil C losses; and then decreased and reached 12 g Cm^{-2} yr^{-1}, 30 years after clear-cut. The simulated early successional trends in NPP and NEP are generally consistent with a variety of chronosequence simulations of recently clear-cut forests of the PNW [e.g., *Grant et al*., 2007; *Turner et al*., 2004; *Janisch and Harmon*, 2002]. *Grant et al*. [2007] simulated the change in NEP with forest age in a coastal Douglas-fir forest of the PNW and found that NEP decreased (−620 g Cm^{-2} yr^{-1}) at the onset of the disturbance, then became positive, and peaked (approximately 450 g Cm^{-2} yr^{-1}) approximately 18 years after clear-cut. *Janisch and Harmon* [2002] found that post-clear-cut NEP was negative (−250 g Cm^{-2} yr^{-1}) at the onset of clear-cut, increased and became positive 12–14 years after disturbance, and then peaked at approximately 200 g Cm^{-2} yr^{-1}, 50–70 years after disturbance. However, post-clear-cut NEP values simulated by VELMA for WS10 were less than simulated NEP values of other PNW forests and were negative

Table 4. Streamflow and Nutrient Losses Modeling Skills for the Postharvest Period[a] (1975–2008)

	Streamflow and Nutrient Losses Modeling Skills		
Parameter	Correlation Coefficient R^2	Baseline Adjusted Modified Index of Agreement d'_1	Root-Mean-Square Error
Streamflow	0.91	0.82	3.34
NH_4 loss	0.7	0.52	0.02
NO_3 loss	0.47	0.18	0.64
DON loss	0.82	0.5	0.06
DOC loss	0.94	0.84	0.19

[a]Observed daily streamflow from 1975 to 2008; observed triweekly NH_4 (mg Nm^{-2} yr^{-1}), NO_3 (mg Nm^{-2} yr^{-1}), and DON (mg Nm^{-2} yr^{-1}) losses from 1979 to 2007; and observed triweekly DOC (mg Cm^{-2} yr^{-1}) losses from 2001 to 2007.

for a shorter period of time. This difference might be in part due to (1) the simulated removal of slash and woody debris from the clear-cut watershed, which has been found to hastened the recovery of simulated NEP [*Grant et al*., 2007], and (2) VELMA's simplified assumption of a single stand instead of complex regenerating stands, which has been found to introduce a bias toward lower NEP [*Grant et al*., 2007].

6. Conclusion

[32] The ecohydrological model presented here, VELMA, provides a relatively simple, spatially distributed framework for assessing the effects of changes in climate, land use (harvest, fire, etc.), and land cover on hydrological, ecological, and biogeochemical processes within watersheds. VELMA was used as a heuristic tool to provide process-level insights into the impact of forest fire and harvest on catchment biogeochemical fluxes at a small intensively studied catchment in the PNW (WS10), details that would be difficult or impossible to capture through experimentation or observation alone. Moreover, VELMA provides a framework for understanding how limited supplies of available N tightly constrain ecosystem responses (production and accumulation of biomass, NEP, etc.) to major disturbances in WS10, and perhaps, more generally for Douglas-fir dominated forests in the western Oregon Cascades of the PNW. Although the impact of disturbances on catchment biogeochemical fluxes has already been investigated in earlier experimental studies [e.g., *Sollins and McCorison*, 1981; *Sollins et al*., 1980; *Vitousek and Reiners*, 1975; *Vitousek et al*., 1979; among others], the interaction of hydrological and biogeochemical processes represented in VELMA provides additional insight into how feedbacks among the cycles of C, N, and water regulate N supplies. The main insights from this exercise include the following:

[33] 1. Following harvest, nutrient losses from the terrestrial system to the stream were tightly constrained by the hydrological cycle, particularly at the hillslope scale. Losses of NH_4, DON, and DOC to the stream were primarily driven by wet-season rain events that were large enough to generate hydrologic connectivity and flushing of nutrients down hillslopes. In contrast, losses of nitrate to the stream were less predictable, owing to complex spatial and temporal patterns of nitrification and denitrification (e.g., hillslope versus riparian zone).

[34] 2. Gaseous losses of C and N to the atmosphere, following disturbance, were primarily driven by high soil water content, high SOC decomposition, and low N uptake. Specifically, postdisturbance increase in soil moisture and nitrate availability enhanced the anaerobic process of soil denitrification and increased N_2-N_2O emissions to the atmosphere, whereas postdisturbance increase in SOC decomposition enhanced soil heterotrophic respiration and increased CO_2 emission to the atmosphere.

[35] Although this exercise is intended to illustrate how a process-based ecohydrological modeling framework can provide useful insights into ecosystem responses to disturbance, we emphasize that VELMA uses a simplified modeling approach with comparatively few parameters and data input requirements. Although one of our objectives is to provide a framework that can be efficiently scaled up to much larger watersheds and time scales of interest to land managers and policymakers, it is important to examine a few of the simplifying assumptions we made to conduct this study. The following five points are a brief summary of watershed characteristics relevant to biogeochemical processes and nutrient export that are not addressed in this study.

[36] (1) *Multiple species*: Aboveground and belowground biomass as well as the different species that usually populate a forested watershed is simplified by using an aggregated biomass pool. However, coexisting grass, shrubs, and trees compete for nutrients, moisture, and energy (i.e., interspecific competition) [*Rozzell*, 2003; *West and Chilcote*, 1968]. As a result, species tend to be spatially distributed based on their tolerance to local conditions (soil water content, nutrient availability, energy, among others) [*Van Breemen et al*., 1997]. *Gholz et al*. [1985] found that, a few years after clear-cut, the riparian zone in WS10 had the greatest annual increase in biomass and was dominated by *Aralia californica*, whereas *Senecio sylvaticus* dominated the midlands. This spatial variability in biomass accumulation and species affects biogeochemical process such as nutrient uptake and nutrient fixation, leading to higher nutrient uptakes in the lowlands, which, in turn, reduces nutrient losses to the stream. Incorporating multiple species and their interactions in VELMA would reduce the amount of simulated nitrogen that reaches the stream and would allow exploration of postharvest successional changes in the spatial and temporal distribution of species within watersheds.

[37] (2) *In-stream processes*: Our simulations assume that the stream nutrient concentration reflects forest processes and do not include in-stream processes. In-stream processes are responsible for temporary retention and recycling of nutrients by a wide variety of physical, chemical, and biological mechanisms [*Bilby and Likens*, 1980; *Triska et al*., 1984; *Wallace and Benke*, 1984] such as adsorption mechanisms, algae uptake, benthic release, denitrification, and decomposition, among others [*Bernot and Dodds*, 2005]; and they are usually important for large watersheds and short time scales [*Tague and Band*, 2004]. *Peterson et al*. [2001] found that in-stream processes such as nitrification rates in a third-order stream in the HJA are responsible for the removal of 40% of the ammonium losses that reach the stream. Although the incorporation of in-stream processes in VELMA is beyond the scope of this paper, doing so would provide a more accurate representation of mechanisms controlling catchment-scale N export. In its present configuration, VELMA is calibrated to provide a best fit for observed N export at a particular stream sampling point, typically a stream gauging station. Thus, in-stream processes affecting measured concentrations of dissolved N are implicitly included in this model calibration. Consequently, an explicit treatment of in-stream processes would require recalibration of the terrestrial processes controlling N transport to the stream.

[38] (3) *N fixation*: VELMA does not include the effect of N fixation on plant biomass dynamics and N cycling. N fixation can be an important source of N input into PNW coniferous forests [*Sollins et al*., 1980] and usually occurs during early successional stages following disturbance,

when N fixing plants and microorganisms tend to be more abundant [*Rastetter et al*., 2001]. However, this simplification is acceptable for WS10, given the low abundance of N fixers in the young, postharvest forest. *Gholz et al*. [1985] found that post-clear-cut N fixers such as red alder (*Alnus rubra*) and snowbush (*Ceanothus veluntinus*) were sparse and limited to the riparian zone of WS10.

[39] (4) *Controls on dissolved organic matter*: VELMA does not explicitly model processes that control the retention and loss of dissolved organic matter. In a field study conducted in HJA, *Yano et al*. [2004, 2005] found that the net retention of soil dissolved organic matter are controlled by the relative magnitude of hydrophobic and hydrophilic acid fractions as well as by the litter quality. For example, *Yano et al*. [2005] found that DON production from root litters is an order of magnitude higher than other litter types (i.e. needle and wood). Other studies have shown that anions such as sulfate and phosphate can impact retention of DOC in forest soils by competing with DOC for adsorption sites within the soil matrix [*Vance and David*, 1992]. Although the incorporation of the chemical processes discussed above in VELMA is beyond the scope of this paper, doing so would provide a more accurate representation of mechanisms controlling catchment-scale DON and DOC production and export. In its present configuration, VELMA is calibrated to provide a best fit for observed DON and DOC exports. Thus, the chemical processes affecting measured concentrations of DON and DOC are implicitly included in this model calibration. Consequently, an explicit treatment of the chemical processes would require recalibration of the terrestrial processes controlling DON and DOC transport to the stream.

[40] (5) *Soil spatial heterogeneity*: Soil texture and depth vary spatially within WS10 [*McGuire et al*., 2007; *Ranken*, 1974; *Sayama and McDonnell*, 2009]. However, deriving high-resolution and catchment wide soil texture and depth maps from, typically, a small number of point measurements, is, at best, uncertain. Instead, we assume uniform loam soil texture and uniform depth to bedrock of 2 m to reflect, more or less, average conditions in the catchment [*Ranken*, 1974]. Although a sensitivity analysis on the impact of the spatial distribution of soil texture and soil depth on streamflow dynamics would certainly provide insights into catchment dynamics, it is beyond the scope of this paper.

[41] For some applications, the explicit treatment of these processes may be needed. However, it must be recognized that such added processes come at the cost of increased model complexity, computational efficiency, and applicability to larger spatial and temporal scales. These are important tradeoffs to consider, given that data needed to implement complex models are not generally available.

Appendix A: Model Description

[42] VELMA is a spatially distributed ecohydrology model that accounts for hydrological and biogeochemical processes within watersheds. The model simulates daily to century-scale changes in soil water storage, surface and subsurface runoff, vertical drainage, carbon and nitrogen cycling in plants and soils, as well as transport of nutrients from the terrestrial landscape to the streams. VELMA consists of multilayered soil column models that communicate with each other through the downslope lateral transport of water and nutrients (Figure (A1)). Each soil column model consists of three coupled submodels: a hydrological model, a soil temperature model, and a plant-soil model. Described below are the soil temperature and plant-soil component of the model. The hydrological component was described in a previous manuscript [*Abdelnour et al*., 2011]. First, we describe the soil column model and then place this soil column within a catchment framework.

A1. Soil Column Framework

[43] We employ a multilayered soil column as a fundamental hydrologic and ecological unit. The soil column consists of n soil layers (Figures (A2) and (A3)). Soil water balance, soil subsurface temperature, and soil C and N pools are computed for each layer.

A1.1. Soil Temperature Model

[44] The soil temperature model first simulates the ground surface temperature (GST) from the available mean surface air temperature (T_a) in the presence of snow cover.

[45] The ground surface temperature is calculated as follows:

$$\mathrm{GST}(t) = T_a \times \exp^{\left(\frac{\mathrm{SD}(t)}{\lambda_{\mathrm{snow}}}\right)}, \tag{A1}$$

where SD(t) is the snow depth (mm) at time t, and λ_{snow} is the seasonal damping depth for snow that is approximately equal to 670 mm [*Hillel*, 1998] for a snowpack of density 300 kg m^{-3}. In this model, snow is an insulative material that only attenuates the mean surface air temperature signal [*Cheng et al*., 2010]. The attenuation of the T_a signal is assumed proportional to the depth of the snowpack [*Cheng et al*., 2010]. As a result, during snow free periods, the ground surface temperature is assumed equal to the mean surface air temperature: SD = 0, GST = T_a.

[46] Subsurface heat transfer is then simulated using the analytical solution of the one-dimensional heat-conduction equation [*Carslaw and Jaeger*, 1959; *Hillel*, 1998].

[47] The subsurface soil temperature in layer i is calculated as follows:

$$T_{s,i}(d_i,t) = \overline{\mathrm{GST}} + \left(\mathrm{GST}(t-\phi(d_i,t)) - \overline{\mathrm{GST}}\right) \times \exp^{\left(-\frac{d_i}{\lambda(t)}\right)} \qquad i = 1,2\ldots n, \tag{A2}$$

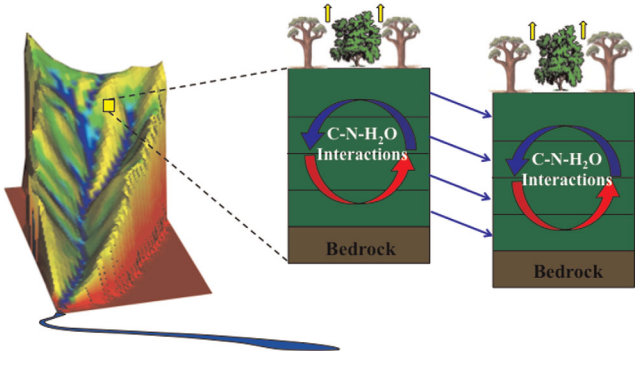

Figure A1. Conceptual catchment modeling framework using multilayered soil columns.

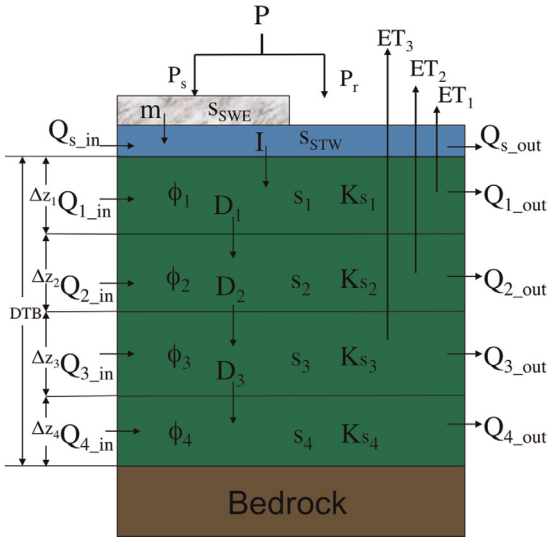

Figure A2. The soil column hydrological framework consists of a four-layered soil column, a standing water layer, and a snow layer. DTB is the soil column depth to bedrock. Δz_i, Ks_i, ϕ_i, and s_i are the thickness, the saturated hydraulic conductivity, the soil porosity, and the soil water storage of layer i, respectively; P, P_s, and P_r are the precipitation, snow, and rain, respectively; m is the snowmelt, and s_{SWE} is the snow water equivalent depth; I is the infiltration, and s_{STW} is the standing water amount; Q_s is the surface runoff; and Q_i, D_i, and ET_i, are the subsurface runoff, the drainage and the ET of layer i, respectively.

where $\overline{\mathrm{GST}}$ is the annual mean soil temperature (°C), d_i is the soil depth to the middle of layer i (mm), $\phi(d_i, t)$ is the phase lag of $T_{s,i}$ relative to GST at depth d_i:

$$\phi(d_i, t) = \left(\frac{d_i}{\lambda(t)} \times \frac{360}{(2\pi)}\right) \qquad i = 1, 2, \ldots n, \tag{A3}$$

and $\lambda(t)$ is the damping depth of the soil (mm), defined as the characteristic depth at which the temperature signal is attenuated to $1/e$ of the GST. $\lambda(t)$ is a function of the thermal properties of the soil and the frequency of the temperature fluctuation:

$$\lambda(t) = \left(\frac{2D_h(t)}{w}\right)^{\frac{1}{2}}, \tag{A4}$$

where $D_h(t)$ is the time-dependent thermal diffusivity of the soil ($\mathrm{mm^2\ d^{-1}}$) and is a function of the simulated soil moisture $\left(\frac{s_i}{s_i^{\max}}\right)$ [*De Vries*, 1975]. For each layer i of the soil column,

$$\begin{aligned} D_h(t) &= \left(19.45 \times 10^{-3}\right) \times \left(\frac{S_i}{S_i^{\max}}\right) + 2 \times 10^{-3} \\ &\text{for} \left(\frac{S_i}{S_i^{\max}}\right) < 0.18 \\ D_h(t) &= \left(-4.055 \times 10^{-3}\right) \times \left(\frac{S_i}{S_i^{\max}}\right) + 6.23 \times 10^{-3} \\ &\text{for} \left(\frac{S_i}{S_i^{\max}}\right) \geq 0.18 \quad i = 1, 2, \ldots n, \end{aligned} \tag{A5}$$

and w is the frequency of annual temperature fluctuation ($\mathrm{d^{-1}}$):

$$w = \frac{2\pi}{365}. \tag{A6}$$

A1.2. Plant-Soil Model

[48] The plant-soil model simulates ecosystem carbon storage and the cycling of carbon and nitrogen between a plant biomass layer and the active soil pools (Figure (A3)). Specifically, the model simulates the interaction among plant biomass (B), SOC including humus and detritus (SOC), plant available soil nitrogen (N) including DON and DIN, as well as DOC. The DIN pool is divided into an ammonium ($\mathrm{NH_4}$) and nitrate ($\mathrm{NO_3}$) pool. B, SOC, $\mathrm{NH_4}$, $\mathrm{NO_3}$, DON, and DOC pools are updated at each time step. For an n-layer soil model ($i = 1, 2, \ldots, n$):

$$\frac{\mathrm{d}B}{\mathrm{d}t} = \left[\left(\sum_{i=1}^{n} \frac{r_i \mu_i \delta_{\mathrm{NH_4}} \mathrm{NH_{4,i}}}{\mathrm{NH_{4,i}} kn}\right)\left(\sum_{i=1}^{n} \frac{r_i \mu_i \delta_{\mathrm{NO_3}} \mathrm{NO_{3,i}}}{\mathrm{NH_{3,i}} kn}\right)\right] \mathrm{WS} \left(\frac{s_i}{s_i^{\max}}\right) B - m, \tag{A7}$$

$$\frac{\mathrm{dSOC}_i}{\mathrm{d}t} = r_i m(B) B - \nu_i\left(T_{s,i}, s_i\right) \mathrm{SOC}_i, \tag{A8}$$

$$\begin{aligned} \frac{d\mathrm{NH_{4,i}}}{\mathrm{d}t} = {} & n_{\mathrm{in}} - r_i \mu_i \delta_{\mathrm{NH_4}} f_M\left(\mathrm{NH_{4,i}}\right) \mathrm{WS}\left(\frac{s_i}{s_i^{\max}}\right) B \\ & + (1 - q) \mathrm{SOC}_i \nu_i\left(T_{s,i}, s_i\right) - \mathrm{Nit}_i - \zeta_v\left(\mathrm{NH_{4,i}}\right) \\ & + \zeta_v\left(\mathrm{NH_{4,i-1}}\right) + \zeta_{l_{\mathrm{in}}}\left(\mathrm{NH_{4,i}}\right) - \zeta_{l_{\mathrm{out}}}\left(\mathrm{NH_{4,i}}\right), \end{aligned} \tag{A9}$$

$$\begin{aligned} \frac{d\mathrm{NO_{3,i}}}{\mathrm{d}t} = {} & \mathrm{Nit}_i - r_i \mu_i \delta_{\mathrm{NO_3}} f_M\left(\mathrm{NO_{3,i}}\right) \mathrm{WS}\left(\frac{s_i}{s_i^{\max}}\right) B - \mathrm{Den}_i \\ & - \zeta_v\left(\mathrm{NO_{3,i}}\right) + \zeta_v\left(\mathrm{NO_{3,i-1}}\right) + \zeta_{l_{\mathrm{in}}}\left(\mathrm{NO_{3,i}}\right) \\ & - \zeta_{l_{\mathrm{out}}}\left(\mathrm{NO_{3,i}}\right), \end{aligned} \tag{A10}$$

$$\begin{aligned} \frac{\mathrm{dDOC}_i}{\mathrm{d}t} = {} & \alpha_{\mathrm{CN}} c_d \mathrm{SOC}_i \ \nu_i\left(T_{s,i}, s_i\right) - \zeta_v(\mathrm{DOC}_i) + \zeta_v(\mathrm{DOC}_{i-1}) \\ & + \zeta_{l_{\mathrm{in}}}(\mathrm{DOC}_i) - \zeta_{l_{\mathrm{out}}}(\mathrm{DOC}_i), \end{aligned} \tag{A11}$$

$$\begin{aligned} \frac{\mathrm{dDON}_i}{\mathrm{d}t} = {} & q \mathrm{SOC}_i \ \nu_i\left(T_{s,i}, s_i\right) - \zeta_v(\mathrm{DON}_i) + \zeta_v(\mathrm{DON}_{i-1}) \\ & + \zeta_{l_{\mathrm{in}}}(\mathrm{DON}_i) - \zeta_{l_{\mathrm{out}}}(\mathrm{DON}_i), \end{aligned} \tag{A12}$$

where $m(B)$ is the plant mortality rate ($\mathrm{d^{-1}}$); r_i and μ_i are the biomass root fraction and the uptake rate function ($\mathrm{d^{-1}}$) in layer i, respectively; $\delta_{\mathrm{NH_4}}$ and $\delta_{\mathrm{NO_3}}$ are the fractions of nitrogen uptake from the ammonium and nitrate pool, respectively; SOC_i, $\mathrm{NH_{4,i}}$, $\mathrm{NO_{3,i}}$, DOC_i, and DON_i are the SOC, ammonium, nitrate, DOC, and DON pools in layer i, respectively ($\mathrm{g\ Nm^{-2}}$ or $\mathrm{g\ Cm^{-2}}$); kn ($\mathrm{g\ Nm^{-2}}$) is the Michaelis-Menten calibration parameter; $\mathrm{WS}\left(s_i/s_i^{\max}\right)$ is the water stress function; $\nu_i\left(T_{s,i}, s_i\right)$ is a first-order SOC decomposition rate ($\mathrm{d^{-1}}$); n_{in} is the atmospheric input of wet and dry nitrogen deposition ($\mathrm{g\ Nm^{-2}\ d^{-1}}$); $(1 - q) \times \mathrm{SOC}_i \times \nu_i\left(T_{s,i}, s_i\right)$ is the flux of carbon into the

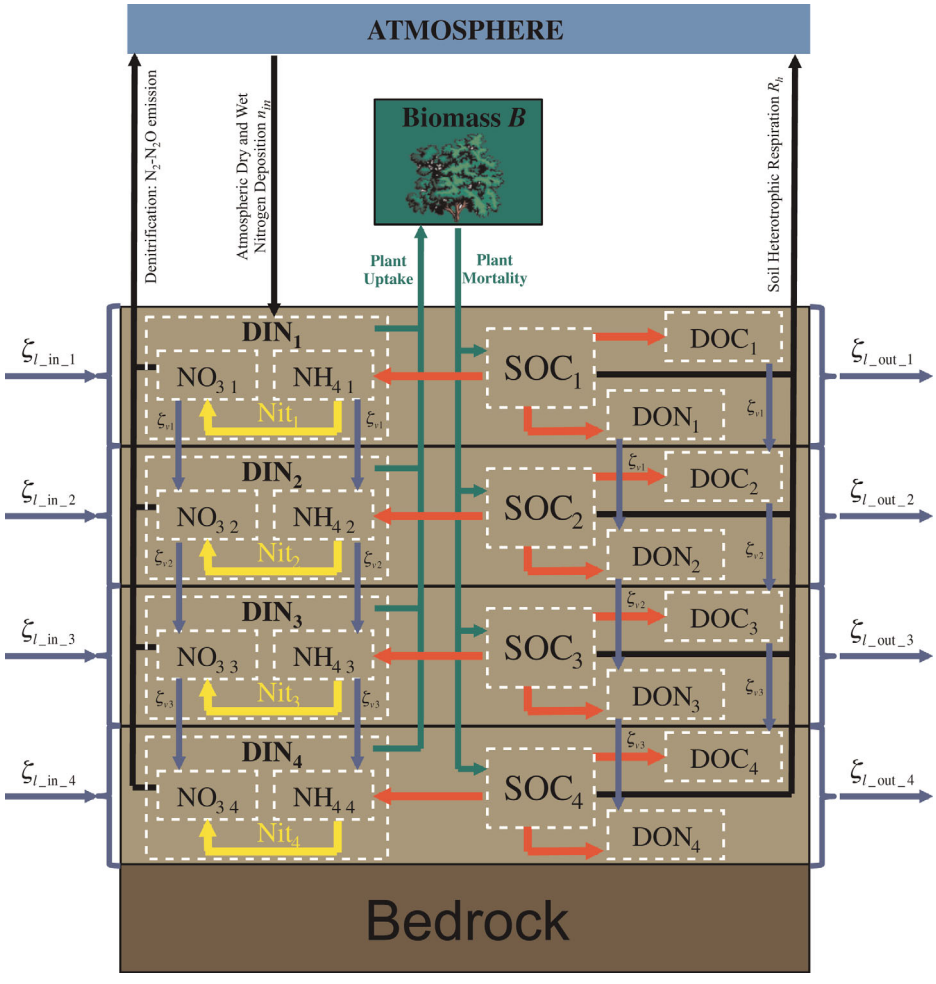

Figure A3. The soil column biogeochemical framework simulates ecosystem carbon storage and the cycling of carbon and N between a plant biomass layer and a four-layered soil column. B is the aboveground and belowground plant biomass. DIN_i is the DIN pool in layer i. The DIN pool consists of a nitrate pool and an ammonium pool and constitutes the available soil nitrogen for plant uptake. Nit_i is the ammonium nitrification into nitrate in layer i (yellow arrows). The NO_3 pool decomposes through denitrification, which releases N_2-N_2O gases into the atmosphere. n_{in} is the atmospheric wet and dry nitrogen deposition and is accounted for in the first layer nitrogen pool. DON_i and DOC_i are the DON and DOC pool in layer i, respectively. SOC_i is the SOC pool in layer i. Plant mortality is a source of carbon into the SOC pool. The SOC pool decomposes through soil microbial activity into DON, DOC, and NH_4 (red arrows). Soil heterotrophic respiration R_h from SOC decomposition in each layer i is released into the atmosphere. NO_3, NH_4, DON, and DOC are soluble and transported through water drainage from layer i to layer $i+1$ and through subsurface runoff from layer i of the soil column to layer i of a downslope soil column (blue arrows). $\zeta_{v,i}$ is the vertical loss of nutrients from layer i to layer $i+1$. $\zeta_{l\_in\_i}$ and $\zeta_{l\_out\_i}$ are the lateral soluble nutrients in and out of layer i, respectively.

ammonium pool due to SOC decomposition in layer i (g Nm^{-2} d^{-1}); $q \times SOC_i \times \nu_i(T_{s,i}, s_i)$ is the flux of carbon into the DON pool due to SOC decomposition in layer i (g Nm^{-2} d^{-1}); $\alpha c_d \times SOC_i \times \nu_i(T_{s,i}, s_i)$ is the flux of carbon from the SOC pool into the DOC pool within layer i (g Cm^{-2} d^{-1}); $f_M(NH_{4,i})$ and $f_M(NO_{3,i})$ are the Type II Michaelis-Menten functions for ammonium and nitrate uptake in layer i, respectively; Nit_i and Den_i are the ammonium nitrification (g Nm^{-2} d^{-1}) and nitrate denitrification (g Nm^{-2} d^{-1}) amounts in layer i, respectively; $\zeta_v(NH_{4i})$, $\zeta_v(NO_{3i})$, $\zeta_v(DOC_i)$, and $\zeta_v(DON_i)$ are the NH_4 (g Nm^{-2} d^{-1}), NO_3 (g Nm^{-2} d^{-1}), DOC (g Cm^{-2} d^{-1}), and DON (g Nm^{-2} d^{-1}) losses through vertical transport of water (i.e., drainage) from layer i to layer $i+1$; $\zeta_{l\_out}(NH_{4i})$, $\zeta_{l\_out}(NO_{3i})$, $\zeta_{l\_out}(DOC_i)$, and $\zeta_{l\_out}(DON_i)$ are the NH_4 (g Nm^{-2} d^{-1}), NO_3 (g Nm^{-2} d^{-1}), DOC (g Cm^{-2} d^{-1}), and DON (g Nm^{-2} d^{-1}) losses out of layer i, through lateral transport of water (i.e., subsurface runoff) from layer i of the soil column to layer i of a downslope soil column or toward the stream; $\zeta_{l\_in}(NH_{4i})$, $\zeta_{l\_in}(NO_{3i})$, $\zeta_{l\_in}(DOC_i)$, and $\zeta_{l\_in}(DON_i)$ are the NH_4, NO_3, DOC, and DON fluxes into layer i, through lateral transport of water (i.e., subsurface

runoff) from layer i of an upslope soil column; α is the C:N ratio for plants and soils and is currently assumed constant for the entire simulations; c_d is the fraction of carbon that is not lost to the atmosphere due to soil heterotrophic respiration.

A1.2.1. Atmospheric Nitrogen Deposition

[49] Atmospheric inputs of wet and dry nitrogen deposition are assumed to affect only the first soil layer and to be temporally distributed throughout the year as a function of precipitation:

$$n_{\text{in}} = \overline{n}_{\text{in}} \times \frac{(P_r + m)}{P_{\text{am}}}, \tag{A13}$$

where $\overline{n}_{\text{in}}$ is the long-term average annual wet and dry nitrogen deposition (g Nm^{-2} yr^{-1}), P_r is the rain (mm d^{-1}), m is the snowmelt (mm d^{-1}), and P_{ann} is the long-term average annual precipitation (mm yr^{-1}).

A1.2.2. Michaelis-Menten Functions

[50] The Type II Michaelis-Menten functions are used to limit NH_4 and NO_3 uptake.

$$\begin{aligned} f_M(\text{NH}_{4i}) &= \frac{\text{NH}_{4i}}{\text{NH}_{4i} + kn} \\ f_M(\text{NO}_{3i}) &= \frac{\text{NO}_{3i}}{\text{NO}_{3i} + kn} \qquad i = 1, 2 \ldots n, \end{aligned} \tag{A14}$$

$$m(B) \begin{cases} \left(\dfrac{(m_a \times B)_{mb} \times m_c}{B} \right) & \text{for } B < B_{st} \\ m_{st} & \text{for } B \geq B_{st} \end{cases}, \tag{A15}$$

where m_a, m_b, and m_c are the mortality rate parameters; m_{st} is the equilibrium mortality rate of old-growth stands (d^{-1}); and B_{st} is the biomass value at equilibrium for an old-growth stand (g Nm^{-2} or g Cm^{-2}/α).

A1.2.4. Plant Uptake

[52] Plant uptake rate is assumed to increase with increasing stand age (S_{age}), reach a maximum value for young stand, and then decrease and reach equilibrium value for mature/old-growth stand [*Acker et al.*, 2002; *Waring and Franklin*, 1979].

$$\mu_i = \begin{cases} \mu_{\min} + 1.44 \times \left(\dfrac{W_{k_1}}{W_{\lambda_1}} \right) \times \left(\dfrac{S_{\text{age}}}{W_{\lambda_1} \times S_{\text{age}}^{\max}} \right)^{w_{k_1} - 1} \times \exp \left(\dfrac{S_{\text{age}}}{W_{\lambda_1} \times S_{\text{age}}^{\max}} \right)^{w_{k_1}} & \text{for } S_{\text{age}} \leq S_{\text{age}}^{\max} \\ \mu_{\text{st}} + \left(\dfrac{W_{k_1}}{W_{\lambda_2}} \right) \times \left(\dfrac{S_{\text{age}}}{W_{\lambda_2} \times S_{\text{age}}^{\max}} \right)^{w_{k_2} - 1} \times \exp \left(\dfrac{S_{\text{age}}}{W_{\lambda_2} \times S_{\text{age}}^{\max}} \right) & \text{for } S_{\text{age}} > S_{\text{age}}^{\max} \end{cases} \qquad i = 1, 2, \ldots n, \tag{A16}$$

where $\mu_{\min}$ is the minimum uptake rate of plant (d^{-1}); μ_{st} is the steady-state/equilibrium value of plant uptake (d^{-1}); $S_{\text{age}}^{\max}$ is the stand age for which plant uptake is the highest (days); and W_{k_1}, W_{λ_1}, W_{k_2} and W_{λ_2} are the Weibull distribution parameters to calibrate.

A1.2.5. Water Stress Function

[53] The water stress function varies between 0 and 1 and is proportional to the soil layer water saturation. The water stress function limits plant growth (i.e., plant nutrient uptake capacity), as soil layer wetness approaches zero or saturation.

$$\text{WS}\left(\frac{S_i}{S_i^{\max}} \right) = \begin{cases} 0.002154 \times \exp^{\left(15.3511 \times \left(\frac{S_i}{S_i^{\max}} \right) \right)} & \text{for } \left(\dfrac{S_i}{S_i^{\max}} \right) < \text{WS}^{\min} \\ 1 & \text{for } \text{WS}^{\min} \leq \left(\dfrac{S_i}{S_i^{\max}} \right) \leq \text{WS}^{\max} \\ 2.44141 \times \exp^{\left(-1.116 \times \left(\frac{S_i}{S_i^{\max}} \right) \right)} & \text{for } \left(\dfrac{S_i}{S_i^{\max}} \right) > \text{WS}^{\max} \end{cases} \qquad i = 1, 2, \ldots n, \tag{A17}$$

A1.2.3. Plant Mortality

[51] Plant mortality rate is simulated as a function of plant biomass. *Acker et al.* [2002] found that biomass mortality increases slowly with age for young stand, until it reaches the mortality of mature and old-growth stands. In VELMA, plant mortality is assumed to increase exponentially with biomass and to reach a steady state value for mature/old-growth stands.

where $WS^{\min}$ and $WS^{\max}$ are the minimum and maximum soil layer water saturation values between which water stress function has no effect on plant nutrient uptake, respectively.

A1.2.6. Biomass Root Fraction

[54] Biomass root fraction distribution with depth follows *Gale and Grigal* [1987] model of vertical root distribution:

$$r_i = 1 - \beta^{d_i} - \sum_{j=1}^{i} r_j, \qquad i = 1, 2, \ldots n, \tag{A18}$$

where β is a fitted "extinction coefficient" that depends on the vegetation type.

A1.2.7. Vertical Transport of Nutrient

[55] Vertical transport of nutrients within the soil column is a function of the vertical water drainage and the size of the nutrient pool in layer i:

$$\varsigma_v(\mathrm{NH}_{4i}) = qf_{\mathrm{NH}_4} \times \frac{D_i}{S_i} \times \mathrm{NH}_{4i} \qquad i = 1, 2 \ldots n, \tag{A19}$$

$$\varsigma_v(\mathrm{NO}_{3i}) = qf_{\mathrm{NO}_3} \times \frac{D_i}{S_i} \times \mathrm{NO}_{3i} \qquad i = 1, 2 \ldots n, \tag{A20}$$

$$\varsigma_v(\mathrm{DON}_i) = qf_{\mathrm{DON}} \times \frac{D_i}{S_i} \times \mathrm{DON}_i \qquad i = 1, 2 \ldots n, \tag{A21}$$

$$\varsigma_v(\mathrm{DOC}_i) = qf_{\mathrm{DOC}} \times \frac{D_i}{S_i} \times \mathrm{DOC}_i \qquad i = 1, 2 \ldots n, \tag{A22}$$

where D_i (mm d^{-1}) is the vertical water drainage from layer i to layer $i+1$; S_i (mm) is the amount of water in layer i; and qf_{NH_4},qf_{NO_3},qf_{DON}, and qf_{DOC} are the maximum fractions of NH_4, NO_3, DON, and DOC pools, respectively, that can be lost through transport of water.

A1.2.8. SOC Decomposition

[56] SOC decomposition rate varies with environmental factors such as soil temperature [*Katterer et al*., 1998; *Lloyd and Taylor*, 1994; *Rustad and Fernandez*, 1998] and soil moisture [*Davidson et al*., 2000] and is based on the process-based TEM presented by *Raich et al*. [1991]. Soil moisture impacts SOC decomposition rate via moisture availability in dry soil and via oxygen availability in wet soil, such as

$$v_i\left(T_{s,i}, s_i\right) = k_c \times F_c^{\mathrm{temp}}\left(T_{s,i}\right) \times F_c^{\mathrm{moisture}}\left(\frac{s_i}{S_i^{\max}}\right), \qquad i = 1, 2, \ldots n, \tag{A23}$$

$$F_c^{\mathrm{temp}}\left(T_{s,i}\right) = 0.00442 \times e^{\left(0.0693 \times T_{s,i}\right)}, \quad i = 1, 2, \ldots n, \tag{A24}$$

$$F_c^{\mathrm{moisture}}\left(\frac{S_i}{S_i^{\max}}\right) = 0.8 \times M_{\mathrm{sat}}^{A} + 0.2, \quad i = 1, 2, \ldots n, \tag{A25}$$

$$A = \left(\frac{\left(100 \times \left(\frac{S_i}{S_i^{\max}}\right)\right)^{ma_1} - \left(\frac{S_i}{S_i^{\max}}\right)_{\mathrm{opt}}^{ma_1}}{\left(\frac{S_i}{S_i^{\max}}\right)_{\mathrm{opt}}^{ma_1} - 100^{ma_1}} \right)^2, \qquad i = 1, 2, \ldots n, \tag{A26}$$

where k_c (d^{-1}) is the potential decomposition rate determined by model calibration; $F_c^{\mathrm{temp}}\left(T_{s,i}\right)$ relates the microbial activity rate to changes in soil temperature (Equation 1.13 [*Raich et al*., 1991]); $F_c^{\mathrm{moisture}}\left(S_i/S_i^{\max}\right)$ defines the impact of soil moisture on decomposition (Equation 1.14b [*Raich et al*., 1991]); M_{sat} is a parameter that determines the value of $F_c^{\mathrm{moisture}}\left(S_i/S_i^{\max}\right)$ when the soil is saturated (Table A5 [*Raich et al*., 1991]); ma_1 is a shape parameter defining the skewness of the curve (Table A5 [*Raich et al*., 1991]); $\left(S_i/S_i^{\max}\right)_{\mathrm{opt}}$ is the optimal soil wetness value for which carbon decomposition is maximal; and $F_c^{\mathrm{temp}}\left(T_{s,i}\right)$ and $F_c^{\mathrm{moisture}}\left(S_i/S_i^{\max}\right)$ vary between the values of 0 and 1.

A1.3. Nitrification Rate

[57] Nitrification is the biological oxidation of ammonium into nitrite and subsequently nitrate under aerobic conditions. Nitrification occurs naturally in the environment and is carried out by autotrophic bacteria. Soil nitrification rates depend on a number of environmental factors such as soil ammonium level [*Smart et al*., 1999], soil moisture [*Davidson et al*., 1993], soil temperature [*Malhi and McGill*, 1982], and soil pH [*DeGroot et al*., 1994]. In VELMA, nitrification is simulated using similar equations to the generalized model of N_2 and N_2O production of *Parton et al*. [1996, 2001]. Soil nitrification rate is assumed to (1) increase exponentially with soil temperature ($F_N^{\mathrm{temp}}\left(T_{s,i}\right)$; Figure 2b [*Parton et al.,* 1996]), (2) increase as soil layer water saturation reaches optimal value for bacterial decomposition and then decrease rapidly as soil layer reaches saturation ($F_N^{\mathrm{moisture}}\left(S_i/S_i^{\max}\right)$; Figure 2a [*Parton et al*., 1996]), (3) decrease exponentially as soil layer acidity (pH_i) increases ($F_N^{\mathrm{moisture}}\left(S_i/S_i^{\max}\right)$; Figure 2c [*Parton et al*., 1996]), and (4) be limited by the amounted of ammonium available for nitrification.

[58] The nitrification rate in layer i is calculated as follows:

$$\mathrm{Nit}_i = K_N^{\max} \times F_N^{\mathrm{temp}}\left(T_{s,i}\right) \times F_N^{\mathrm{acidity}}(\mathrm{pH}_i) \times F_N^{\mathrm{moisture}}\left(\frac{S_i}{S_i^{\max}}\right) \times f_m(\mathrm{NH}_{4i}) \times \mathrm{NH}_{4i} \qquad i = 1, 2 \ldots n, \tag{A27}$$

$$F_N^{\mathrm{temp}}\left(T_{s,i}\right) = -0.06 + 0.13 \times e^{\left(0.07 \times T_{s,i}\right)} \qquad i = 1, 2 \ldots n, \tag{A28}$$

$$F_N^{\mathrm{acidity}}(pH_i) = 0.56 + \frac{\arctan(\pi \times 0.45 \times (-5 \times \mathrm{pH}_i))}{\pi} \qquad i = 1, 2 \ldots n, \tag{A29}$$

$$F_N^{\mathrm{moisture}}\left(\frac{S_i}{S_i^{\max}}\right) = \left(\frac{\left(\frac{S_i}{S_i^{\max}}\right) - N_b}{N_a - N_b}\right)^{\left(N_d \times \frac{N_b - N_a}{N_a - N_c}\right)} \times \left(\frac{\left(\frac{S_i}{S_i^{\max}}\right) - N_b}{N_a - N_c}\right)^{N_d} \qquad i = 1, 2 \ldots n, \tag{A30}$$

where $K_N^{\max}$ (d^{-1}) is the maximum nitrification rate determined by model calibration; and N_a, N_b, N_c, and N_d are the soil parameters set according to soil texture and described by *Parton et al*. [1996].

A1.4. Denitrification Rate

[59] Denitrification is the biological reduction of nitrate under anaerobic conditions. During denitrification, heterotrophic microbes contribute to the NO_3 reduction into NO_2, NO, and N_2O intermediates and ultimately into molecular

0043-1397/13/2012WR012994

©2012. American Geophysical Union. All Rights Reserved.
0043-1397/13/2012WR012994

nitrogen N_2 lost to the atmosphere. The denitrification process is controlled by environmental factors such as soil nitrate level, soil oxygen availability, and soil labile carbon availability (e^- donor) [*Weier et al*., 1993]. In VELMA, denitrification is simulated using the denitrification submodel of N_2 and N_2O production presented by *Parton et al*. [1996, 2001] and *Del Grosso et al*. [2000]. The rate of denitrification is proportional to the amount of bioavailable SOC level. However, VELMA does not differentiate between labile and nonlabile soil organic matter. Therefore, simulated ecosystem CO_2 loss (soil heterotrophic respiration) is used as a proxy for the amount of bioavailable SOC [*Del Grosso et al*., 2000; *Parton et al*., 1996]. The rate of denitrification increases with decreasing oxygen availability. Oxygen availability is another critical factor not simulated by VELMA but assumed as a function of soil moisture, soil gas diffusivity, and oxygen demand. Gas diffusivity is simulated as a function of soil moisture and soil properties, whereas oxygen demand is a function of the simulated soil heterotrophic respiration [*Del Grosso et al*., 2000; *Parton et al*., 1996]. As a result, soil denitrification rate is simulated as a function of soil saturation $F_D^{\text{moisture}}\left(S_i/S_i^{\max}\right)$ (Equation (A1) [*Parton et al*., 2001]), soil heterotrophic respiration $F_D^{\text{carbon}}\left(CO_{2,i}\right)$ (Figure 1d [*Del Grosso et al*., 2000]), and soil available nitrate $F_D^{\text{nitrate}}(\text{NO}_{3i})$ (Figure 1c [*Del Grosso et al*., 2000]). Currently, VELMA simulates the total denitrification or N_2+N_2O emission without the partition between N_2 and N_2O, such that

$$\text{Den}_i = \min\left[F_D^{\text{carbon}}(CO_{2i}), F_D^{\text{nitrate}}(\text{NO}_{3i})\right] \times F_D^{\text{moisture}}\left(\frac{S_i}{S_i^{\max}}\right) \quad i = 1, 2 \ldots n, \tag{A31}$$

$$F_D^{\text{moisture}}\left(\frac{S_i}{S_i^{\max}}\right) = 0.5 + \frac{\arctan\left(\pi \times 0.6 \times \left(0.1 \times \left(\frac{S_i}{S_i^{\max}}\right)\right) - \vartheta_a\right)}{\pi} \quad i = 1, 2 \ldots n, \tag{A32}$$

$$F_D^{\text{carbon}}\left(CO_{2,i}\right) = 0.1 \times \left(\alpha \times c_d \times \text{SOC}_i \times v_i\left(T_{s,i}, S_i\right)\right)^{1.3} \quad i = 1, 2 \ldots n, \tag{A33}$$

$$F_D^{\text{nitrate}}(\text{NO}_{3i}) = 0.005 \times (\text{NO}_{3i})^{0.57} \quad i = 1, 2 \ldots n, \tag{A34}$$

where $F_D^{\text{carbon}}\left(CO_{2,i}\right)$ and $F_D^{\text{nitrate}}(\text{NO}_{3i})$ represent the maximum possible N gas flux from layer i for a given soil heterotrophic respiration rate and nitrate level, respectively (g Nm^{-2} d^{-1}); ϑ_a is a shape parameter that depends on soil texture; and $F_D^{\text{moisture}}\left(S_i/S_i^{\max}\right)$ varies between 0 and 1.

A2. Watershed Framework

[60] To place the earlier described soil column framework within a catchment framework, the catchment topography is gridded into a number of pixels, with each pixel consisting of one coupled soil column. Soil columns communicate with each other through the downslope lateral transport of water and nutrients. Surface and subsurface runoff are responsible for this lateral transport and link each soil column to the surrounding downslope soil columns. A multiple flow direction method is used where flow and nutrients from one pixel to its eight neighbors is fractionally allocated according to terrain slope [*Freeman*, 1991; *Quinn et al*., 1991]. Moreover, nutrients transported downslope from one soil column to another can be processed through the different submodels in that downslope soil column, or continue to flow downslope, interacting with other soil columns, or ultimately discharging water and nutrients to the stream.

A2.1. Lateral Transport of Nutrients

[61] Lateral transport of nutrients from layer i of an upslope soil column to layer i of a downslope soil column or toward the stream is based on the flow routing information and on terrain slope. As with the vertical transport of nutrients, the lateral transport of nutrient is a function of the lateral runoff and the size of the nutrient pool in layer i. For simplicity, we assume that both surface runoff and layer 1 subsurface runoff impact the nutrient pool in layer 1 of the soil column:

$$\zeta_1(\text{NH}_{4i}) = qf_{\text{NH}_4} \times \frac{Q_i + q_{\text{surf}} \times Q_s}{S_i} \times \text{NH}_{4i} \quad i = 1, 2 \ldots n, \tag{A35}$$

$$\zeta_1(\text{NO}_{3i}) = qf_{\text{NO}_3} \times \frac{Q_i + q_{\text{surf}} \times Q_s}{S_i} \times \text{NO}_{3i} \quad i = 1, 2 \ldots n, \tag{(A36)}$$

$$\zeta_1(\text{DON}_i) = qf_{\text{DON}_1} \times \frac{Q_i + q_{\text{surf}} \times Q_s}{S_i} \times \text{DON}_i \quad i = 1, 2 \ldots n, \tag{A37}$$

$$\zeta_1(\text{DOC}_i) = qf_{\text{DOC}_1} \times \frac{Q_i + q_{\text{surf}} \times Q_s}{S_i} \times \text{DOC}_i \quad i = 1, 2 \ldots n, \tag{A38}$$

with $q_{\text{surf}} = \begin{cases} 1 & \text{for} \quad i = 1 \\ 0 & \text{for} \quad i = 2, 3 \ldots n \end{cases}$,

where Q_i (mm d^{-1}) is the lateral subsurface runoff from layer i (Equation (A16) [*Abdelnour et al*., 2011]; and Q_s (mm d^{-1}) is the surface runoff that impact the nutrients

Table B1. Model Parameter Values Used to Simulate the Biogeochemical Processes of WS10 in the HJA

Parameters	Definition	Value	References
λ_{snow}	Seasonal damping depth for snow (mm)	670	*Hillel* [1998]
$\overline{\text{GST}}$	Annual mean soil temperature (°C)	8.5	*Sollins and McCorison* [1981]
Kn	Michaelis-Menten calibration parameter (g Nm^{-2})	0.1	Calibrated
δ_{NO_3}	Fraction of nitrogen uptake from the nitrate pool	0.3	*Rygiewicz and Bledsoe* [1986], *Kamminga-van Wijk and Prins* [1993]
δ_{NH_4}	Fraction of nitrogen uptake from the ammonium pool	0.7	*Rygiewicz and Bledsoe* [1986], *Kamminga-van Wijk and Prins* [1993]
α_{CN}	C:N ratio for plants and soils	50	*Sollins and McCorison* [1981]
c_d		0.004	Calibrated

Table B1. (continued)

Parameters	Definition	Value	References
	Fraction of carbon that is not lost to the atmosphere due to the soil heterotrophic respiration		
$\overline{n_{\text{in}}}$	Annual wet and dry deposition of atmospheric N (g Nm^{-2} yr^{-1})	0.2	*Sollins et al*. [1980]
β	Fitted extinction coefficient	0.976	*Jackson et al*. [1996]
q	Fraction of carbon decomposition that feeds into the DON pool	0.015	Calibrated
m_{st}	Steady-state average mortality rate of old-growth forest (yr^{-1})	0.0125	*Lutz and Halpern* [2006]
B_{st}	Average biomass value for an old-growth forest (g Nm^{-2})	42,350	*Harmon et al*. [2004], *Sollins et al*. [1980]
m_a	Mortality rate parameter	1.55	Fixed a priori
m_b	Mortality rate parameter	4	Fixed a priori
m_c	Mortality rate parameter	1E−14	Fixed a priori
$\mu_{\min}$	Minimum uptake rate of vegetation after disturbance (yr^{-1})	0.20	Fixed a priori
μ_{st}	Steady state value of plant uptake (yr^{-1})	0.25	Calibrated
$S_{\text{age}}^{\max}$	Stand age for which plant uptake is the highest (years)	35	*Luyssaert et al*. [2008]
W_{k1}	Weibull distribution parameter for plant uptake	1.60	Fixed a priori
$W_{\lambda 1}$	Weibull distribution parameter for plant uptake	1.70	Fixed a priori
W_{k2}	Weibull distribution parameter for plant uptake	0.95	Fixed a priori
$W_{\lambda 2}$	Weibull distribution parameter for plant uptake	0.85	Fixed a priori
$WS^{\min}$	Lower limit of soil water saturation, below which plant uptake is reduced (%)	40	Fixed a priori
$WS^{\max}$	Upper limit of soil water saturation, above which plant uptake is reduced (%)	80	Fixed a priori
k_c	Potential carbon decomposition rate (vegetation dependent; yr^{-1})	0.45	Calibrated
M_{sat}	Parameter that determines the value $F_N^{\text{moisture}}\left(s_i/s_i^{\max}\right)$	0.25	*Raich et al*. [1991]
ma_1	Shape parameter defining the skewness of the $F_N^{\text{moisture}}\left(s_i/s_i^{\max}\right)$ curve	0.14	*Raich et al*. [1991]
$\left({}^{s_i}/_{S}{}^{\max}\right)_o$	Optimal soil wetness for which decomposition is maximal	40%	*Alexander* [1977]
pH	Average pH value for the soils in WS10	4.5	*Chaeir et al*. [2009]
$K_N^{\max}$	Maximum nitrification rate (d^{-1})	0.15	*Parton et al*. [2001]
N_a	Soil moisture function parameter for ammonium nitrification	0.4	*Parton et al*. [1996]
N_b	Soil moisture function parameter for ammonium nitrification	1.7	*Parton et al*. [1996]
N_c	Soil moisture function parameter for ammonium nitrification	3.22	*Parton et al*. [1996]
N_d	Soil moisture function parameter for ammonium nitrification	0.007	*Parton et al*. [1996]
ϑ_a	Soil moisture function shape parameter	5.0	*Del Grosso et al*. [2000]
qf_{NH_4}	Maximum fraction of NH_4 pool that can be lost through transport of water	0.12	Calibrated
qf_{NO_3}	Maximum fraction of NH_4 pool that can be lost through transport of water	0.04	Calibrated
qf_{DON}	Maximum fraction of NH_4 pool that can be lost through transport of water	0.02	Calibrated
qf_{DOC}	Maximum fraction of NH_4 pool that can be lost through transport of water	0.06	Calibrated

pools in layer 1 (Equation (A18) [*Abdelnour et al*., 2011]).

Appendix B

[62] Appendix B describes the list of parameters used in the model. Table B1 includes the parameters definitions, values and references.

[63] **Acknowledgments.** The information in this document has been funded in part by the U.S. Environmental Protection Agency. It has been subjected to the agency's peer and administrative review, and it has been approved for publication as an EPA document. Mention of trade names or commercial products does not constitute endorsement or recommendation for use. This research was additionally supported in part by the following NSF grants 0439620, 0436118, and 0922100. We thank Sherri Johnson, Barbara Bond, Suzanne Remillard, Theresa Valentine, and Don Henshaw for invaluable assistance in accessing and interpreting various H.J. Andrews LTER data sets used in this study. Sherri Johnson also provided helpful comments on an earlier draft. Data for streamflow, stream chemistry, and climate were provided by the HJA Research Program, funded by the National Science Foundation's Long-Term Ecological Research Program (DEB 08-23380), U.S. Forest Service Pacific Northwest Research Station, and Oregon State University.

References

Abdelnour, A., M. Stieglitz, F. Pan, and R. McKane (2011), Catchment hydrological responses to forest harvest amount and spatial pattern, *Water Resour. Res.*, *47*, W09521, doi:10.1029/2010WR010165.

Acker, S., C. Halpern, M. Harmon, and C. Dyrness (2002), Trends in bole biomass accumulation, net primary production and tree mortality in Pseudotsuga menziesii forests of contrasting age, *Tree Physiol.*, *22*(2–3), 213.

Agee, J. K. (1990), The historical role of fire in Pacific Northwest forests, edited by J. D.Walstad, S. R. Radosevich, and D. V. Sandberg, Natural and prescribed fire in Pacific Northwest forests, Oregon State University Press, Corvallis, Oregon, USA.

Agee, J. (1994), Fire and weather disturbances in terrestrial ecosystems of the eastern Cascades, Gen. Tech. Rep. PNW-GTR-320, U.S. For. Serv., Pac. Northwest Res. *Stn, Portland, Oreg*.

Alexander, M. (1977), *Introduction to Soil Microbiology*, 2nd ed., Wiley, New York.

Alila, Y., and J. Beckers (2001), Using numerical modelling to address hydrologic forest management issues in British Columbia, Hydrol. *Processes*, *15*(18), 3371–3387.

Amaranthus, M., H. Jubas, and D. Arthur (1989), Stream shading, summer streamflow and maximum water temperature following intense wildfire in headwater streams, in *Proceedings of the Symposium on Fire and Watershed Management, Sacramento, California*, edited by N. H. Berg, Gen. Tech. Rep. PSW-109, pp. 75–78, U.S. Dept. of Agric., For. Serv., Pac. Southwest For. and Range Exp. Stn., Berkeley, Calif., 26–28 Oct. 1988.

Bernot, M., and W. Dodds (2005), Nitrogen retention, removal, and saturation in lotic ecosystems, *Ecosystems*, *8*(4), 442–453.

Beschta, R. L. (1990), *Effects of fire on water quantity and quality, in Natural and Prescribed Fire in Pacific Northwest Forests*, edited by J. D. Walstad, S. R. Radosevich, and D. V. Sandberg, pp. 219–232, Oreg. State Univ. Press, Corvallis, Oreg.

Beschta, R., M. Pyles, A. Skaugset, and C. Surfleet (2000), Peakflow responses to forest practices in the western Cascades of Oregon, USA, *J. Hydrol*., *233*(1–4), 102–120.

Bilby, R., and G. Likens (1980), Importance of organic debris dams in the structure and function of stream ecosystems, *Ecology*, *61*(5), 1107–1113.

Binkley, D., P. Sollins, R. Bell, D. Sachs, and D. Myrold (1992), Biogeochemistry of adjacent conifer and alder-conifer stands, *Ecology*, *73*(6), 2022–2033.

Bormann, F., G. Likens, D. Fisher, and R. Pierce (1968), Nutrient loss accelerated by clear-cutting of a forest ecosystem, *Science*, *159*(3817), 882.

Bosch, J., and J. Hewlett (1982), A review of catchment experiments to determine the effect of vegetation changes on water yield and evapotranspiration, *J. Hydrol.*, *55*(1–4), 3–23.

Cairns, M., and K. Lajtha (2005), Effects of succession on nitrogen export in the west-central Cascades, Oregon, *Ecosystems*, *8*(5), 583–601.

Carslaw, H., and J. Jaeger (1959), *Conduction of Heat in Solids*, 2nd ed., Oxford Univ. Press, New York.

Chaeir, G., M. Fernandes, D. Myrold and P. Bottomley (2009), Comparative resistance and resilience of soil microbial communities and enzyme in adjacent native forest and agricultural soils, *Soil Microbiol.*, *58*(2), 414–424.

Cheng, Y., M. Stieglitz, and F. Pan (2010), A simple method to evolve daily ground temperatures from surface air temperatures in snow dominated regions, *J. Hydrometeorol.*, *11*, 1395–1404.

Creed, I., L. Band, N. Foster, I. Morrison, J. Nicolson, R. Semkin, and D. Jeffries (1996), Regulation of nitrate-N release from temperate forests: A test of the N flushing hypothesis, *Water Resour. Res.*, *32*(11), 3337–3354.

Daly, C., and W. McKee (2011), *Meteorological data from benchmark stations at the Andrews Experimental Forest, Long-Term Ecol. Res.*, For. Sci. Data Bank, Corvallis, Oreg. [Database]. [Available at http://andrewsforest.oregonstate.edu/data/abstract.cfm?dbcode=MS001, accessed16 July 2011.].

Davidson, E., P. Matson, P. Vitousek, R. Riley, K. Dunkin, G. Garcia-Mendez, and J. Maass (1993), Processes regulating soil emissions of NO and N_2O in a seasonally dry tropical forest, *Ecology*, *74*(1), 130–139.

Davidson, E., L. Verchot, J. Cattânio, I. Ackerman, and J. Carvalho (2000), Effects of soil water content on soil respiration in forests and cattle pastures of eastern Amazonia, *Biogeochemistry*, *48*(1), 53–69.

De Vries, D. A. (1975), Heat transfer in soils, in *Heat and Mass Transfer in the Biosphere*, edited by D. A. de Vries and N. F. Afgan, pp. 528, Scripta, New York.

DeGroot, C., A. Vermoesen, and O. Cleemput (1994), Laboratory study of the emission of NO and N_2O from some Belgian soils, Environ. *Monit. Assess.*, *31*(1), 183–189.

Del Grosso, S., W. Parton, A. Mosier, D. Ojima, A. Kulmala, and S. Phongpan (2000), General model for N_2O and N_2 gas emissions from soils due to denitrification, *Global Biogeochem. Cycles*, *14*(4), 1045–1060.

Dingman, S. (1994), *Physical Hydrology*, Prentice Hall, Upper Saddle River, NJ.

Dyrness, C. (1973), Early stages of plant succession following logging and burning in the western Cascades of Oregon, *Ecology*, *54*(1), 57–69.

Franklin, J. F., and R. T. T. Forman (1987), Creating landscape patterns by forest cutting: Ecological consequences and principles, *Landscape Ecol.*, *1*(1), 5–18.

Fredriksen, R. (1975), *Nitrogen, phosphorus and particulate matter budgets of five coniferous forest ecosystems in the western Cascades Range, Oregon, Ph.D. dissertation, 71 pp.*, Oreg. State Univ., Corvallis.

Freeman, T. (1991), Calculating catchment area with divergent flow based on a regular grid, *Comput. Geosci.*, *17*(3), 413–422.

Gale, M. R., and D. F. Grigal (1987), Vertical root distributions of northern tree species in relation to successional status, *Can. J. For. Res.*, *17*(8), 829–834.

Gholz, H. L., G. M. Hawk, A. Campbell, K. Cromack Jr., and A. T. Brown (1985), Early vegetation recovery and element cycles on a clear-cut watershed in western Oregon, *Can. J. For. Res.*, *15*(2), 400–409.

Giesen, T. W., S. S. Perakis, and K. Cromack Jr. (2008), Four centuries of soil carbon and nitrogen change after stand-replacing fire in a forest landscape in the western Cascade Range of Oregon, *Can. J. For. Res.*, *38*(9), 2455–2464.

Grant, G., S. Lewis, F. Swanson, J. Cissel, and J. McDonnell (2008), Effects of forest practices on peak flows and consequent channel response: A state-of-science report for western Oregon and Washington, Gen. Tech. Rep. PNW-GTR-760, 76 pp., USDA For. Serv., Pac. Northwest Res. Stn., *Portland, Oreg*.

Grant, R., N. Juma, J. Robertson, R. Izaurralde, and W. B. Mcgill (2001), Long-term changes in soil carbon under different fertilizer, manure, and rotation—Testing the mathematical model ecosys with data from the Breton plots, Soil Sci. Soc. *Am. J.*, *65*(1), 205–214.

Grant, R., T. Black, E. Humphreys, and K. Morgenstern (2007), Changes in net ecosystem productivity with forest age following clearcutting of a coastal Douglas-fir forest: Testing a mathematical model with eddy covariance measurements along a forest chronosequence, *Tree Physiol.*, *27*(1), 115.

Grier, C., and R. Logan (1977), Old-growth Pseudotsuga menziesii communities of a western Oregon watershed: Biomass distribution and production budgets, *Ecol. Monogr.*, *47*(4), 373–400.

Grier, C. C. (1975), Wildfire effects on nutrient distribution and leaching in a coniferous ecosystem, *Can. J. For. Res.*, *5*(4), 599–607.

Griffiths, R., and A. Swanson (2001), Forest soil characteristics in a chronosequence of harvested Douglas-fir forests, *Can. J. For. Res.*, *31*(11), 1871–1879.

Halpern, C., and T. Spies (1995), Plant species diversity in natural and managed forests of the Pacific Northwest, *Ecol. Appl.*, *5*, 913–934.

Harmon, M., K. Bible, M. Ryan, D. Shaw, H. Chen, J. Klopatek, and X. Li (2004), Production, respiration, and overall carbon balance in an old-growth Pseudotsuga-Tsuga forest ecosystem, *Ecosystems*, 7(5), 498–512.

Harmon, M. E., and B. Marks (2002), Effects of silvicultural practices on carbon stores in Douglas-fir western hemlock forests in the Pacific Northwest, USA: Results from a simulation model, *Can. J. For. Res.*, *32*(5), 863–877.

Harmon, M. E., W. K. Ferrell, and J. F. Franklin (1990), Effects on carbon storage of conversion of old-growth forests to young forests, *Science*, *247*(4943), 699–701.

Harr, R., and F. M. McCorison (1979), Initial effects of clearcut logging on size and timing of peak flows in a small watershed in western Oregon, *Water Resour. Res.*, *15*(1), 90–94, doi:10.1029/WR1015i1001p00090.

Harr, R., A. Levno, and R. Mersereau (1982), Streamflow changes after logging 130-year-old Douglas fir in two small watersheds, *Water Resour. Res.*, *18*(3), 637–644, doi:610.1029/WR1018i1003p00637.

Helvey, J. (1980), Effects of a north central Washington wildfire on runoff and sediment production, *J. Am. Water Resour. Assoc.*, *16*(4), 627–634.

Hibbert, A. (1966), Forest treatment effects on water yield, in *Proceedings of a National Science Foundation Advanced Science Seminar, International Symposium on Forest Hydrology*, edited by W. E. Sopper and H. W. Lull, pp. 527–543, Pergamon, New York.

Hicke, J. A., G. P. Asner, E. S. Kasischke, N. H. F. French, J. T. Randerson, G. James Collatz, B. J. Stocks, C. J. Tucker, S. O. Los, and C. B. Field (2003), Postfire response of North American boreal forest net primary productivity analyzed with satellite observations, *Global Change Biol.*, *9*(8), 1145–1157.

Hillel, D. (1998), Environmental Soil Physics, Academic, *San Diego, Calif.*

Ice, G. G., D. G. Neary, and P. W. Adams (2004), Effects of wildfire on soils and watershed processes, *J. For.*, *102*(6), 16–20.

Jackson, R. B., J. Canadell, J. Elheringer, H. A. Mooney, O. E. Sala, and E. D. Schulze (1996), A global analysis of root distributions for terrestrial biomes, *Oecologia*, *108*, 389–411.

Janisch, J., and M. Harmon (2002), Successional changes in live and dead wood carbon stores: Implications for net ecosystem productivity, *Tree Physiol.*, *22*(2–3), 77.

Johnson, S., and R. Fredriksen (2010), Long-term precipitation and dry deposition chemistry concentrations and fluxes: Andrews Experimental Forest rain collector samples, Long-Term Ecol. Res., For. Sci. Data Bank, Corvallis, Oreg. [Database]. [Available at http://andrewsforest.oregonstate.edu/data/abstract.cfm?dbcode=CP002, accessed 31 Aug. 2011].

Johnson, S., and R. Fredriksen (2011), Long-term stream chemistry concentrations and fluxes: Small watershed proportional samples in the Andrews Experimental Forest, Long-Term Ecol. Res., For. Sci. Data Bank, Corvallis, Oreg. [Database]. [Available at http://andrewsforest.oregonstate.edu/data/abstract.cfm?dbcode=CF002, accessed 18 July 2011.].

Johnson, S., and J. Rothacher (2009), Stream discharge in gaged watersheds at the Andrews Experimental Forest, Long-Term Ecol. Res., For. Sci. Data Bank, Corvallis, Oreg. [Database]. [Available at http://andrewsforest.oregonstate.edu/data/abstract.cfm?dbcode=HF004, accessed 16 July 2011.].

Jones, J. A. (2000), Hydrologic processes and peak discharge response to forest removal, regrowth, and roads in 10 small experimental basins, western Cascades, Oregon, *Water Resour. Res.*, *36*(9), 2621–2642, doi:2610.1029/2000WR900105.

Jones, J. A., and G. E. Grant (1996), Peak flow responses to clear-cutting and roads in small and large basins, western Cascades, Oregon, *Water Resour. Res.*, *32*(4), 959–974.

Jones, J. A., and D. A. Post (2004), Seasonal and successional streamflow response to forest cutting and regrowth in the northwest and eastern United States, *Water Resour. Res.*, *40*(5), W05203, doi:05210.01029/02003WR002952.

Kamminga-van Wijk, C., and H. Prins (1993), The kinetics of NH_4^+ and NO_3^-, *Plant Soil*, *151*, 91–96.

Katterer, T., M. Reichstein, O. Andren, and A. Lomander (1998), Temperature dependence of organic matter decomposition: A critical review using literature data analyzed with different models, *Biol. Fert. Soils*, *27*(3), 258–262.

Keppeler, E. T., and R. R. Ziemer (1990), Logging effects on streamflow: Water yield and summer low flows at Caspar Creek in northwestern California, *Water Resour. Res.*, *26*(7), 1669–1679.

Kirchner, J. W. (2003), A double paradox in catchment hydrology and geochemistry, *Hydrol. Processes*, *17*, 871–874.

Langford, K. (1976), Change in yield of water following a bushfire in a forest of Eucalyptus regnans, *J. Hydrol.*, *29*(1–2), 87–114.

Law, B., P. Thornton, J. Irvine, P. Anthoni, and S. Van Tuyl (2001), Carbon storage and fluxes in ponderosa pine forests at different developmental stages, *Global Change Biol.*, *7*(7), 755–777.

Lee, J., I. K. Morrison, J. D. Leblanc, M. T. Dumas, and D. A. Cameron (2002), Carbon sequestration in trees and regrowth vegetation as affected by clearcut and partial cut harvesting in a second-growth boreal mixedwood, *For. Ecol. Manage.*, *169*(1–2), 83–101.

Lloyd, J., and J. Taylor (1994), On the temperature dependence of soil respiration, *Funct. Ecol.*, *8*(3), 315–323.

Lutz, J. A., and C. B. Halpern (2006), Tree mortality during early forest development: A long-term study of rates, causes, and consequences, *Ecol. Monogr.*, *76*(2), 257–275.

Luyssaert, S., E. Schulze, A. Borner, A. Knohl, D. Hessenmoller, B. Law, P. Ciais, and J. Grace (2008), Old-growth forests as global carbon sinks, *Nature*, *455*(7210), 213–215.

Malhi, S., and W. McGill (1982), Nitrification in three Alberta soils: Effect of temperature, moisture and substrate concentration, Soil Biol. *Biochem.*, *14*(4), 393–399.

Martin, W. C., and R. D. Harr (1989), Logging of mature Douglas-fir in western Oregon has little effect on nutrient output budgets, *Can. J. For. Res.*, *19*(1), 35–43.

McGuire, K. J., M. Weiler, and J. J. McDonnell (2007), Integrating tracer experiments with modeling to assess runoff processes and water transit times, Adv. *Water Resour.*, *30*(4), 824–837, ISSN 0309-1708, 10.1016/j.advwatres.2006.07.004.

McKane, R., E. Rastetter, G. Shaver, K. Nadelhoffer, A. Giblin, J. Laundre, and F. Chapin III (1997), Climatic effects on tundra carbon storage inferred from experimental data and a model, *Ecology*, *78*(4), 1170–1187.

Means, J., P. MacMillan, and K. Cromack (1992), Biomass and nutrient content of Douglas-fir logs and other detrital pools in an old-growth forest, Oregon, U.S.A., *Can. J. For. Res. (Print)*, *22*(10), 1536–1546.

Millennium Ecosystem Assessment (2005), Ecosystems and Human Well-being: Biodiversity Synthesis. World Resources Institute, Washington, DC.

Mitchell, S. R., M. E. Harmon, and K. E. B. O'Connell (2009), Forest fuel reduction alters fire severity and long-term carbon storage in three Pacific Northwest ecosystems, *Ecol. Appl.*, *19*(3), 643–655.

Moore, R., and S. Wondzell (2005), Physical Hydrology in the Pacific Northwest and the effects of forest harvesting: A review, *J. Am. Water Resour. Assoc.*, *41*, 753–784.

Neary, D., K. Ryan, and L. DeBano (2005), Fire effects on soil and water, Gen. Tech. Rep. RMRS-GTR-42, USDA For. *Serv., Rocky Mt. Res. Stn*.

Parton, W., B. McKeown, V. Kirchner, and D. Ojima (1992), CENTURY Users Manual, Colorado State University, NREL Publication, Fort Collins, Colo.

Parton, W., A. Mosier, D. Ojima, D. Valentine, D. Schimel, K. Weier, and A. Kulmala (1996), Generalized model for N_2 and N_2O production from nitrification and denitrification, *Global Biogeochem. Cycles*, *10*(3), 401–412.

Parton, W., E. Holland, S. Del Grosso, M. Hartman, R. Martin, A. Mosier, D. Ojima, and D. Schimel (2001), Generalized model for NO_x and N_2O emissions from soils, *J. Geophys. Res.—Atmos.*, *106*(D15), 17,403–17,420.

Peng, C., H. Jiang, M. Apps and Y. Zhang (2002), Effects of harvesting on carbon and nitrogen dynamics of boreal forests in central Canada: A process model simulation, *Ecol. Model.*, *155*(2–3), 177–189.

Peterson, B., W. Wollheim, P. Mulholland, J. Webster, J. Meyer, J. Tank, E. Marti, W. Bowden, H. Valett, and A. Hershey (2001), Control of nitrogen export from watersheds by headwater streams, *Science*, *292*(5514), 86.

Quinn, P., K. Beven, P. Chevallier, and O. Planchon (1991), Prediction of hillslope flow paths for distributed hydrological modelling using digital terrain models, *Hydrol. Processes*, *5*(1), 59–79.

Raich, J., E. Rastetter, J. Melillo, D. Kicklighter, P. Steudler, B. Peterson, A. Grace, B. Moore III, and C. Vorosmarty (1991), Potential net primary productivity in South America: Application of a global model, *Ecol. Appl.*, *1*(4), 399–429.

Ranken, D. W. (1974), *Hydrologic properties of soil and subsoil on a steep, forested slope, Master's dissertation, 117 pp*., Oreg. State Univ., Corvallis.

Rastetter, E., P. Vitousek, C. Field, G. Shaver, D. Herbert, and G. Gren (2001), Resource optimization and symbiotic nitrogen fixation, *Ecosystems*, *4*(4), 369–388.

Rothacher, J. (1965), Streamflow from small watersheds on the western slope of the Cascade Range of Oregon, *Water Resour. Res.*, *1*, 125–134, doi:110.1029/WR1001i1001p00125.

Rozzell, L. R. (2003), Species pairwise associations over nine years of secondary succession: Assessing alternative explanations and successional mechanisms, Master's dissertation, *Utah State Univ., Logan, Utah*.

Rustad, L., and I. Fernandez (1998), Soil warming: Consequences for foliar litter decay in a spruce-fir forest in Maine, USA, Soil Sci. Soc. *Am. J.*, *62*(4), 1072.

Rygiewicz, P., and C. Bledsoe, 1986, Effects of pretreatment conditions on ammonium and nitrate uptake by Douglas-fir seedlings, *Tree Physiol.*, *1*, 145–150.

Santantonio, D., R. Hermann, and W. Overton (1977), *Root biomass studies in forest ecosystems, Pedobiologia, Bd. 17, S. 1–31, Pap. 957, For. Res. Lab., Sch. of For*. Oreg. State Univ., Corvallis, Oreg.

Sayama, T. and J. J. McDonnell (2009), A new time-space accounting scheme to predict stream water residence time and hydrograph source components at the watershed scale, *Water Resour. Res.*, *45*, W07401, doi:10.1029/2008WR007549.

Schmidt, J., W. Seiler, and R. Conrad (1988), Emission of nitrous oxide from temperate forest soils into the atmosphere, *J. Atmos. Chem.*, *6*(1), 95–115.

Smart, D., J. Stark, and V. Diego (1999), Resource limitations to nitric oxide emissions from a sagebrush-steppe ecosystem, *Biogeochemistry*, *47*(1), 63–86.

Smithwick, E., M. Harmon, S. Remillard, S. Acker, and J. Franklin (2002), Potential upper bounds of carbon stores in forests of the Pacific Northwest, *Ecol. Appl.*, *12*(5), 1303–1317.

Sollins, P., and F. M. McCorison (1981), Nitrogen and carbon solution chemistry of an old growth coniferous forest watershed before and after cutting, *Water Resour. Res.*, *17*(5), 1409–1418, doi:1410.1029/WR1017i1005p01409.

Sollins, P., C. Grier, F. McCorison, K. Cromack Jr., R. Fogel, and R. Fredriksen (1980), The internal element cycles of an old-growth Douglas-fir ecosystem in western Oregon, *Ecol. Monogr.*, *50*(3), 261–285.

Sollins, P., K. Cromack Jr., F. Mc Corison, R. Waring, and R. Harr (1981), Changes in nitrogen cycling at an old-growth Douglas-fir site after disturbance, *J. Environ. Qual.*, *10*(1), 37.

Spies, T. A., J. F. Franklin, and T. B. Thomas (1988), Coarse woody debris in Douglas-fir forests of western Oregon and Washington, *Ecology*, *69*(6), 1689–1702.

Stednick, J. (1996), Monitoring the effects of timber harvest on annual water yield, *J. Hydrol.*, *176*(1–4), 79–95.

Stednick, J. D. (2008), *Hydrological and Biological Responses to Forest Practices: The Alsea Watershed Study*, Springer, New York.

Stieglitz, M., J. Shaman, J. McNamara, V. Engel, J. Shanley, and G. Kling (2003), An approach to understanding hydrologic connectivity on the hillslope and the implications for nutrient transport, *Global Biogeochem. Cycles*, *17*(4), 1105.

Storck, P., L. Bowling, P. Wetherbee, and D. Lettenmaier (1998), Application of a GIS-based distributed hydrology model for prediction of forest harvest effects on peak stream flow in the Pacific Northwest, *Hydrol. Processes*, *12*(6), 889–904.

Tague, C., and L. Band (2000), Simulating the impact of road construction and forest harvesting on hydrologic response, Earth Surf. *Processes Landforms*, *26*(2), 135–151.

Tague, C., and L. Band (2004), RHESSys: Regional hydro-ecologic simulation system—An object-oriented approach to spatially distributed modeling of carbon, water, and nutrient cycling, *Earth Interact*., *8*, 1–42.

Tiedemann, A., T. Quigley, and T. Anderson (1988), Effects of timber harvest on stream chemistry and dissolved nutrient losses in northeast Oregon, *For. Sci.*, *34*(2), 344–358.

Triska, F. J., J. R. Sedell, K. Cromack, S. V. Gregory, and F. M. McCorison (1984), Nitrogen budget for a small coniferous forest stream, *Ecol. Monogr.*, *54*(1), 119–140.

Turner, D. P., M. Guzy, M. A. Lefsky, and T. Van (2003), Effects of land use and fine scale environmental heterogeneity on net ecosystem production over a temperate coniferous forest landscape, *Tellus B*, *55*(2), 657–668.

Turner, D. P., M. Guzy, M. A. Lefsky, W. D. Ritts, S. Van Tuyl, and B. E. Law (2004), Monitoring forest carbon sequestration with remote sensing and carbon cycle modeling, *Environ. Manage.*, *33*(4), 457–466.

Valentine, T., and G. Lienkaemper (2005), 30 meter digital elevation model (DEM) clipped to the Andrews Experimental Forest, Long-Term Ecol. Res., For. Sci. Data Bank, Corvallis, Oreg. [Database]. [Available at http://andrewsforest.oregonstate.edu/data/abstract.cfm?dbcode=GI002, accessed 16 Jul. 2011.].

Van Breemen, N., A. C. Finzi, and C. D. Canham (1997), Canopy tree–soil interactions within temperate forests: Effects of soil elemental composition and texture on species distributions, *Can. J. For. Res.*, *27*(7), 1110–1116.

Van Verseveld, W., J. McDonnell and K. Lajtha (2008), A mechanistic assessment of nutrient flushing at the catchment scale, *J. Hydrol.*, *358*, 268–287.

Vance, G. F., and M. B. David. (1992). Dissolved organic carbon and sulfate sorption by spodosol mineral horizons. *Soil Sci.*, *154*, 136–144.

Vanderbilt, K., K. Lajtha, and F. Swanson (2003), Biogeochemistry of unpolluted forested watersheds in the Oregon Cascades: Temporal patterns of precipitation and stream nitrogen fluxes, *Biogeochemistry*, *62*(1), 87–117.

Vitousek, P. M., J. R. Gosz, C. C. Grier, J. M. Melillo, A. Reiners, and R. L. Todd (1979), Nitrate losses from disturbed ecosystems, *Science*, *204*, 469–474.

Vitousek, P., and W. Reiners (1975), Ecosystem succession and nutrient retention: A hypothesis, *BioScience*, *25*(6), 376–381.

Wallace, J., and A. Benke (1984), Quantification of wood habitat in subtropical coastal plain streams, *Can. J. Fish. Aquat. Sci.*, *41*(11), 1643–1652.

Waring, R., and J. Franklin (1979), Evergreen coniferous forests of the Pacific Northwest, *Science*, *204*(4400), 1380–1386.

Weber, M., and M. Flannigan (1997), Canadian boreal forest ecosystem structure and function in a changing climate: Impact on fire regimes, *Environ. Rev.*, *5*(3–4), 145–166.

Weier, K., J. Doran, J. Power, and D. Walters (1993), Denitrification and the dinitrogen/nitrous oxide ratio as affected by soil water, available carbon, and nitrate, Soil Sci. Soc. *Am. J.*, *57*, 66–72.

West, N. E., and W. W. Chilcote (1968), Senecio sylvaticus in relation to Douglas-fir clear-cut succession in the Oregon Coast Range, *Ecology*, *49*(6), 1101–1107.

Wimberly, M. C. (2002), Spatial simulation of historical landscape patterns in coastal forests of the Pacific Northwest, *Can. J. For. Res.*, *32*(8), 1316–1328.

Wright, C. S., and J. K. Agee (2004), Fire and vegetation history in the eastern Cascade Mountains, *Washington, Ecol.* Appl., *14*(2), 443–459.

Wright, H. E., and M. L. Heinselman (1973), The ecological role of fire in natural conifer forests of western and northern North America: Introduction, *Quat. Res.*, *3*, 319–328.

Wright, P., M. Harmon, and F. Swanson (2002), Assessing the effect of fire regime on coarse woody debris, *USDA For. Serv. Gen. Tech. Rep. PSW-GTR 181*, pp. 621–634.

Yanai, R. D., W. S. Currie, and C. L. Goodale (2003), Soil carbon dynamics after forest harvest: An ecosystem paradigm reconsidered, *Ecosystems*, *6*(3), 197–212.

Yano, Y., K. Lajtha, P. Sollins and B. Caldwell (2004), Chemical and seasonal controls on the dynamics of dissolved organic matter in a coniferous old-growth stand in the Pacific Northwest, *USA, Biogeochemistry*, *71*, 197–223.

Yano, Y., K. Lajtha, P. Sollins and B. Caldwell (2005), Chemistry and dynamics of dissolved organic matter in a temperate coniferous forest on andic soil: Effects of litter quality, *Ecosystems*, *8*, 286–300.